STELLAR POPULATIONS
IN THE D WARI? ELLIPTICAL GALAXY NGC 185

MYUNG GYOON LEE and WENDY L FREEDMAN
Carnegie Observatories
813 Santa Barbara Street
Pasadena, CA 91101

and

BARRY F. MADORE[1]
NASA/IPAC Extragalactic Database
Infrared Processing and Analysis Center
Jet Propulsion Laboratory
California Institute of Technology
Pasadena, CA 91101

ABSTRACT

$BVRI$ CCD photometry of $\sim$ 5,300 stars in the central (2'.2 x 3'.5) area of the dwarf elliptical galaxy NGC 185 in the Local Group is presented. The color-magnitude diagrams of NGC 185 show three distinct stellar populations: (1) a strong red giant branch (RGB) population, the tip of which is found to be at I_{TRGB} = 20.3 $\pm$ 0.2 mag, and $(V - I)_{TRGB}$ = 1.95+ 0.05, (2) an asymptotic giant branch (AGB) located above the tip of the RGB, and (3) a small number of young stars having blue to yellow colors. The reddening of the bright foreground stars has been determined using the $(.B - V) - (V - I)$ diagram to be $E(B - V)$ = 0.19+ O.O3 msg. The distance has been estimated from the I magnitude of the tip of the RGB, giving $(m- M).$ = 23.96 $\pm$0.21 mag for A_I = 0.38 mag, corresponding to 620 $\pm$ 60 kpc. The mean metallicity of the RGB stars has been determined using the median color of the RGB stars at M_I = –3.5 mag, $(V - I)_{-3.5,0}$ = 1.727 mag: giving a mean metallicity of [Fe/H] = – 1.23 $\pm$ 0.16 dex. The dispersion in color at MI = –3.5 mag is A(V – $I)_{-3.5}$ = 0.12 mag, implying a metallicity dispersion of – 1.6< [Fe/H] < –0.9 dex. Surface photometry of the area within R = 50" is also presented, showing that colors get rapidly bluer inside $R \approx$ 10". A V luminosity function for the blue stars has been derived, the slope of which is very similar to that for other nearby galaxies. The AGB stars extend to $M_{bol} \approx$ –5.0 mag, and most of the AGB stars above the tip of the RGB are likely to belong to an intermediate-age population. The bolometric luminosity function of the red giant stars in NGC 185 is found to be very similar to that of M32.

1. INTRODUCTION

NGC 185, a companion to the Andromeda galaxy (M31), is a dwarf elliptical galaxy (dE3pec). Basic information for this galaxy is summarized in Table 1. It has been considered as a peculiar elliptical galaxy, because of the presence of blue stars, dust clouds, HI gas, and a possible supernova remnant in the galaxy. Since Baade (1944) resolved this galaxy into individual stars, many studies have been made of various populations in NGC 185 (e. g., blue stars: Baade 1951, Hedge 1963, 1973; globular clusters: Hedge 1974, Da Costa & Mould 1988; planetary nebulae: Ford *et al.* 1977, Ciardullo *et al.* 1989; RR Lyrae stars: Saha & Hoessel 1990; dust clouds: Hedge 1963, Gallagher & Hunter 1981, Price 1985; Supernova Remnants: Gallagher *et al.* (1984); HI gas: Johnson & Gottesman 1983; CO gas: Wiklind & Rydbeck 1986). Reviews of the Andromeda companions have been given by van den Bergh (1975), Hedge (1989), and Freedman (1992a). However, there has been as yet no study of individual stars in NGC 185 except for the RR Lyrae variables (Saha & Hoessel 1990). Because NGC 185 is located close enough to be resolved into individual stars, it, as well as other dwarf elliptical galaxies in the Local Group, provides an excellent laboratory for the comparison of the stellar populations in dwarf elliptical galaxies beyond the Local Group and for investigating the origin of dwarf galaxies.

In this paper, we present a study of stellar populations in the central area of NGC 185 using $BVRI$ CCD photometry. A brief progress report of this study was given in Lee *et al.* (1992a). This paper is composed as follows: Section 2 describes the observations and data reduction, Section 3 presents the color-magnitude diagrams of NGC 185. Sections 4, 5, and 6 discuss the determination of reddening, distance and metallicity, respectively, Section 7 presents surface photometry of the central area of NGC 185 and derives structural parameters, and Section 8 discusses the properties of stellar populations in NGC 185 in comparison with other galaxies. Finally a summary is given in Section 9.

2. OBSERVATIONS AND DATA REDUCTION

2.1 Observations

$BVRI$ CCD images of the central area of NGC 185 were obtained at the prime focus of the Canada-France-Hawaii 3.5m Telescope on a photometric night, September 21, 1987, using the RCA2 "double density" CCD chip. The chip scale is $0''.205/\text{pixel}$ and the CCD image has 640×1024 pixels, corresponding to 131" x 210". The journal of observations of NGC 185 is given in Table 2. The seeing ranged from 0".6 to 0".8. A description of the standard star reduction for the night has been given in Wilson *et al.* (1990).

Grey scale maps of B, V, and I CCD images are shown in Figures 1 (a), (b) and (c). The B image shows a small number of bright stars scattered over the central area of the galaxy as well as two well-known distinctive dust clouds surrounding the center of the galaxy. The I image is better resolved into stars than the B or V image. A concentration of bright stars is apparent in the central area,

2.2 Data Reduction

Instrumental magnitudes of stars in NGC 185 were obtained using the digital photometry reduction program DoPHOT (Mateo *et* cd. 1990). The errors for the aperture corrections to match the magnitudes from the point-spread-function fitting and the magnitudes from the aperture photometry are 0.024, 0.022, 0.011 and 0.014 mag for B, V, R and I, respectively. The instrumental magnitudes were transformed onto the standard system using the standard stars observed on the same night. The standard star calibration errors are 0.012, 0.018, 0.017, 0.018, and 0.013 mag for V, $(B - V)$, $(R - I)$, $(V - I)$, and I, respectively.

The total number of stars which were measured in at least two colors is $\sim 5,300$. Table 3a lists the photometry of 310 stars with $V < 22$ mag which were measured in all four colors, and Table 3b contains the photometry of 80 blue stars with $(B - V) < 0.6$ msg. The table for the photometry of all the measured stars is available from the

authors upon request. Finding charts for the measured stars are given in Figure 2.

3. COLOR-MAGNITUDE DIAGRAMS OF NGC 185

3.1 General Morphology

Figure 3 displays the color-magnitude diagrams (CMDs) of $\sim$ 5,300 stars in NGC 185 in various combinations of magnitudes *(V* and *I*) and colors *((B – V), (V – I)*, and *(R - I))*. The corresponding mean photometric errors (formal errors from DoPHOT) versus *V* and *I* magnitudes are listed in Table 4.

The CMDS of NGC 185 arc, in general, similar to those for NGC 205, another dwarf elliptical companion of M31 (Lee *et* al. 1992b, 1993a). Interesting features illustrated by the CMDS of NGC 185 are as follows: (1) There is a dominant group of red giant stars, the brightest of which is found at $I \approx 19$ mag and $V \approx 21.2$ msg. This group of red giant stars shows an apparent discontinuity in the number density of stars at $I_{TRGB} \approx$ 20.3 rnag and $(V – I)_{TRGB} \approx 2.0$ mag (see the $I – (V – I)$ diagram in Figure 3(d)), which probably represents the tip of the red giant stars (RGB). Stars located above the discontinuous tip of the RGB are asymptotic giant branch (AGB) stars; and (2) There are a small number of young stars with blue to yellow colors, the brightest of which has $V = 20.45$ mag and (.B – *V) =* –0.14 msg. Such stars were first observed by Baade (1951) who counted blue stars on photographic plates of NGC 185. We are presenting photometry of these blue stars for the first time,

3.2 Galactic Foreground Contamination

We can estimate the contamination by Galactic foreground stars in the CMDS using a model of our Galaxy. The number of Galactic foreground stars in the direction of NGC 185 expected from the model of our Galaxy by Ratnatunga & Bahcall (1985) is given in Table 5. All the stars with $V < 20$ mag and most of the red stars with $20 < V < 21$ mag in Figure 3(a) arc probably foreground stars, whereas the contamination of Galactic foreground stars appears to be negligible fainter than $V > 21$ msg.

4. REDDENING

An accurate measurement of the extinction of NGC 185 is critical to an understanding of the stellar populations in NGC 185, because it is located at relatively low Galactic latitude (b = −14.48 deg) leading to significant extinction.

We have used two methods to estimate the foreground extinction toward NGC 185: (1) the color-color diagram for stars and (2) the neutral hydrogen gas/galaxy counts method. First, the foreground reddening has been estimated using the $(B - V) - (V - I)$ diagram of bright foreground stars in comparison with the intrinsic relations of (1? − V) and $(V - I)$ colors for dwarfs and giant stars (Cousins 1978), as is shown in Figure 4. Only stars with $V < 20$ mag and photometric errors smaller than ±0.05 mag were used for this reddening estimation. The reddening thus determined is $E(B - V) =$ 0.19 ± 0.03 msg. Secondly, the reddening map of our Galaxy based on the HI/galaxy counts method (Burstein & Heiles 1982) provides a foreground reddening value for NGC 185, $E(B - V) = 0.19$ mag, which is fortuitously identical to the first estimate. Using a total-to-selective extinction ratio of $R_V = 3.2$ given in Cardelli et $al.$ (1989, their eq. 2 and 3), the extinction values for other wavelength bands are as follows: $A_V =$ $3.20E(B - V) = 0.61$ mag, $A_B = 4.21E(B - V) = 0.80$ mag, $AR = 2.71E(B - V) = 0.51$ mag, and $AI = 1.98E(B - V) = 0.38$ msg.

The presence of two well-known dust clouds surrounding the center of NGC 185 (see Figure 1(a)) implies that there is probably significant internal extinction in the central part of the galaxy (Hedge 1963, Gallagher & Hunter 1981). No quantitative estimate for the amount of internal extinction in NGC 185 is available. However, Figure 1 suggests that there is negligible internal extinction in the outer area.

5. DISTANCE

5.1 Distance Estimate Using the Tip of the Red Giant Branch

We now estimate the distance to NGC 185 from the I magnitude of the tip of the RGB (hereafter TRGB), using the methods described in Mould & Kristian (1983), Da Costa & Armandroff (1990) and Lee et al. (1993 b).

Since the photometry of the outer area surveyed suffers much less of a crowding problem compared with the inner area (see Figure 1), we have used the photometry of stars located at $R > 40$" for the analysis of the red stars in the following. Figure 5 shows the $I - (V-I)$ diagram for these stars. The mean error bars for the I magnitudes and $(V - I)$ colors are plotted to the left side of the figure. We have derived the I luminosity functions for the RGB and AGB stars located in the entire CCD field and those located at $R > 40$", which are listed in Table 6 and plotted in Figure 6. The turnover around the peak of the luminosity functions is almost certainly due to the incompleteness of the photometry. Figure 6 shows that there is an apparent first discontinuity at $I \approx 20.3 \pm 0.1$ mag which probably represents the TRGB. We have used a standard image-processing edge-detection algorithm in order to formally define the position of the TRGB, as described in Lee et al. (1993 b). This edge-detection algorithm employs the zero-sum Sobel kernel [–2, O, +2] which, when convolved with the luminosity functions, gives a maximum in its output at the luminosity where the count discontinuity is the greatest (shown by the dotted lines in Figure 6). The position of the TRGB thus measured for the stars located at $R > 40$" (Figure 6(a)) is at $I = 20.30 \pm 0.20$ msg. The stars brighter than the TRGB represent the AGB stars. As described in Lee et al. (1993b), the position of the TRGB in these data is not very well-defined. The presence of an AGB population results in a much broader distribution than observed in many other nearby galaxies. In this respect NGC 185 is similar to M32 (Freedman 1989). However, as seen below, the distance obtained agrees well with previous estimates. The median value and dispersion of the color for the TRGB are estimated from the photometry of 128 stars with

$20,25 < I < 20.35$ mag: $(V - I)_{TRGB} = 1.95 \pm 0.03$ mag and $\sigma(V - I)_{TRGB} = 0.36$ mag, leading to $(V - I)_{TRGB,0} = 1.72$ mag, for an adopted reddening of $E(V - I) = 0.23$ msg.

The bolometric magnitude of the TRGB is calculated from the relation $M_{bol} = -0.19[Fe/H] - 3.81$ (Da Costa & Armandroff 1990) adopting a value for the metallicity, $[Fe/H] = -1.23 \pm 0.16$ dex (see Section 6): $M_{bol} = -3.58$ msg. Adopting $BC_I = 0.881 - 0.243(V - I)_{TRGB}$ (Da Costa & Armandroff 1990), we estimate the bolometric correction at I for the TRGB, $BC_I = 0.46$ msg. Then the intrinsic I magnitude of the TRGB is given by $M_I = M_{bol} - BC_I = -4.04$ msg.

Finally, the apparent distance modulus to NGC 185 is obtained: $(m - M)_I = 20.30- (-4.04) = 24.34$ msg. As described in Section 4, the internal extinction is probably negligible in the outer area. Therefore only a foreground extinction correction is made to derive a true distance to NGC 185 from the apparent distance modulus. Adopting a foreground extinction of $A_I = 0.38$ mag, we obtain a value for the true distance modulus of $(m - M)_0 = 23.96 \pm 0.21$ mag (corresponding to a distance of 620 ± 60 kpc). Corresponding apparent distance moduli at different wavelength bands are $(m - M)_B = 24.76$, $(m - M)_V = 24.57$, and $(m - M)_R = 24.48$ msg.

5.2 Comparisons with Previous Estimates

Most of the previous estimates of the distance to NGC 185 were based on the simple assumption that NGC 185 is located at the same distance as M31. The first direct estimate of the distance to NGC 185 was made by Saha & Hoessel (1990). They searched for variables in NGC 185 and discovered 151 RR Lyraes using Gunn g photometry. The mean magnitude of the RR Lyraes in NGC 185 was determined to be $g(RR) = 25.20$ mag, corresponding to $V(RR) = 25.24$ msg. They then derived a distance modulus of $(m - M)_0 = 23,79+ 0.25$ mag under the assumptions: $A_g = 0.68$ mag (corresponding to $A_B = 0.80$ mag) and $M_g(RR) = 0.73 \pm 0.25$ mag (equivalent to $M_V = 0.77$ mag). If the relation between the luminosity and the metallicity of RR Lyraes adopted in Da Costa & Armandroff $(M_V (RR) = 0.17[Fe/H] + 0.82)$ is used for NGC 185 so as to be consistent

with distance estimate using the TRGB in this study, then the absolute V magnitude of RR Lyraes is $M_v = 0.61$ mag for [Fe/H] = -1.23 dex. This value of M_V = 0.61 mag leads us to a distance modulus of $(m - M)_0$ = 24.02 mag, which is in excellent agreement with the value we obtain in this study.

Another distance estimate to NGC 185 has been obtained from the luminosity function of planetary nebulae. However, the small number (4) of planetary nebulae discovered in NGC 185 allowed Ciardullo *et al.* (1989) to derive only an upper limit for the distance, $(m - M)$. = 23.78 mag for $E(B - V)$ = 0.17 msg. This estimate also agrees well with our estimate.

Using the same TRGB method as applied to NGC 185, we obtain, from the data for the TRGB of M31 halo (Mould & Kristian 1986), a value for the distance modulus to M31, $(m - M)_0$ = 24.44 mag (Lee *et al.* 1993b), which is identical to a Cepheid distance based on the multi-band CCD photometry (Madore & Freedman 1991). This result suggests that NGC 185 is closer by ~ 0.5 mag (~ 150 kpc) than M31.

6. METALLICITY

We have measured the mean metallicity and its dispersion for the RGB stars in NGC 185 using the $(V - I)$ colors at $MI = -3.5$ msg. Da Costa & Armandroff (1990) provide a calibration for the metallicity of the RGB using the $(V - I)$ colors at $M_I = -3.0$ mag for Galactic globular clusters. However, this calibration could not be used directly for the case of NGC 185, because the colors of the RGB stars in NGC 185 at $M_I = -3.0$ mag are significantly affected by photometric errors and incompleteness in the photometry. To overcome this limitation, a similar calibration (based on the same data as used by Da Costa & Armandroff) but at the half-magnitude brighter magnitude, $M_I = -3.5$ mag, has been derived by Lee *et al.* (1993b): [Fe/H] = $-12.64 + 12.61(V - I)_{-3.5,0} - 3.33(V - I)^2_{-3.5,0}$.

The median value and dispersion of the color at $MI = -3.5$ mag were derived from

our photometry of 272 stars located outside R = 40" with 20.75 $< I <$ 20.85 mag: $(V - I)_{-3.5}$ = 1.727+ 0.036 and $\sigma(V - I)_{-3.5}$ = 0.279 msg. Adopting a foreground reddening of $E(V - I)$ = 0.233 mag, we obtain $(V - I)_{-3.5,0}$ = 1.494 msg. This estimate yields a value for the mean metallicity [Fe/H] = −1.23 ± 0.16 dex using the equation given above.

The dispersion of the observed color of the RGB stars may be the result of several sources: e.g., photometric errors, metal licity dispersion, age spread, or differential reddening. As argued above, the differential reddening is unlikely to affect the color dispersion of stars located in the outer area. The contribution of the age spread to the $(V - I)$ color in the I versus $(V - I)$ diagram is much smaller than the contribution of the metallicity dispersion (Freedman 1989, Da Costa & Armandroff 1990, Lee *et al.* 1993 b). Therefore the dominant sources for the dispersion of the observed colors of the RGB stars are probably the metallicit y dispersion and the photometric errors.

The mean formal photometric error of $(V - I)$ for 20.75<1<20.85 mag is $\sigma(V - I)$ = 0.125 msg. This value may be an underestimate of the true error, because it does not include the effect of crowding in the photometry. If we take, as a conservative estimate for the mean error, twice the value of the formal estimate, $\sigma(V - I)$ = 0.25 mag, then the intrinsic dispersion of the color is A $(V - I)_{-3.5} = \sqrt{0.28^2 - 0.25^2}$ = 0.12 msg. The metallicity dispersion corresponding to this intrinsic color dispersion is −1.6 < [Fe/H] < −0.9 dex. This size of the metallicity dispersion in NGC 185 is similar to those estimated for NGC 205 (Mould *et al.* 1984) and M32 (Freedman 1989).

The loci for the RGB of Galactic globular clusters with [Fe/H] = -2.2 to -0.7 dex (M15, M2, NGC 1851 and 47 Tut) are displayed in Figure 5 after being shifted according to the distance and reddening of NGC 185. They show clearly how large the dispersion of the metallicity in NGC 185 is.

This large metallicity dispersion in NGC 185 is also indicated by the wide period distribution of the RR Lyraes in Saha & Hoessel (1990). Saha & Hoessel found that the

majority of the RR Lyraes in NGC 185 have periods of 0.3 to 0.8 days. The period distribution is bimodal, having peaks near 0.50 and 0.63 days, which is similar to the case of ω Cen. The wide period distribution of NGC 185 implies that the metallicity ranges from [Fe/H] = -1.0 to -2.0 dex, which is confirmed by our finding of a significant $(V - I)$ color range for the RGB stars.

It is interesting to compare the metallicity of the RGB stars in NGC 185 with that of the globular clusters in NGC 185. Da Costa & Mould (1988) found from the spectroscopic study of five globular clusters in NGC 185 that the metallicity 'of the globular clusters ranges from [Fe/H] = -1.2 to –2.5 dex with a mean value of [Fe/H] $=-1.65 \pm 0.25$ dex. The mean metallicity of the RGB stars is slightly larger than that of globular clusters, which is consistent with previous studies indicating that the colors of halos in elliptical galaxies are redder than that of globular clusters (Harris 1991). The large metallicity dispersion for the RGB stars is consistent with that exhibited by the globular clusters.

7. SURFACE PHOTOMETRY AND STRUCTURAL PARAMETERS

7.1 Surface Photometry

Our CCD frames do not cover the whole of NGC 185, but they are still useful for the study of integrated light and surface brightness profiles for the central area of the galaxy. Integrated and surface photometry of the central area within 50" have been obtained using elliptical apertures with an ellipticity of $\epsilon = 0.25$ and a position angle of 50 deg (see Kent 1987). The photometry has been obtained following the method outlined by Djorgovski (1988) and Lee (1990). The elliptical annulus apertures were divided into eight azimuthal sectors. The integrated brightness is determined from the median value of the eight sectors and the corresponding error is determined from the standard error of the median value. The area of the CCD field is too small to measure reliably the background sky value for the integrated photometry so that we adopted, as the value of

sky intensity, a value $\sim 15\%$ lower than the lowest sky in the CCD frame. Thus we are limited to surface photometry measurements in the inner region of NGC 185 (less than 50"). The photometric error due to the uncertainty in the sky estimation is smaller than 0.05 mag for $R < 50$". The distributions of integrated light and color as well as surface brightness and color profiles are plotted in Figure 7. They show: (a) The $(V - R)$ and $(B - V)$ colors of NGC 185 remain nearly constant beyond $\sim 20''$, while the $(V - I)$ and $(B - I)$ colors get bluer slowly toward the center. This is due to shallower gradient of the I surface brightness profile compared with B, V, and R profiles. It is not clear whether this difference is due to intrinsic properties of NGC 185 or due to uncertainties in our photometry. Better photometry with larger areal coverage is encouraged to resolve this problem; and (b) All the colors become blue very rapidly inside $R = 10$", probably due to the presence of young stars in the central area suggested in the following. We plotted the magnitudes $(V$ and $I)$ and colors $((I? - V)$ and $(V - I))$ of individual stars in NGC 185 against the galacto-centric radius in Figure 8. Colors are plotted for bright stars with $V < 22$ mag to avoid any selection effect due to a varying magnitude limit over galacto-centric radius. Figure 8 shows that there is an excess of blue stars in the central area and that the color variation over the radial distance is almost negligible in the outer area, a result consistent with the surface photometry.

7.2 Comparisons with Previous Photometry

Previous surface photometry of NGC 185 has been published by Hedge (1963), Price (1985), and Kent (1987). Kent (1987) presented Gunn r CCD surface photometry of NGC 185 based on ellipse-fitting. His r photometry is converted to Cousins R photometry by using the approximate relation between Gunn r and Cousins R given by Barsony [1989]: $r = R + 0.038(R - I) + 0.280$. The approximate average $(R - I)$ color of NGC 185 is ~ 0.80 mag (measured in this study), for which we obtain $R = r - 0.31$. A comparison of the R surface brightness profiles from our study and Kent's shows excellent agreement between the two, as is shown in Figure 7(a). The slight difference shown for

the region at 3" $< R < 18$" is likely due to the presence of the dust clouds in NGC 185, because our photometry is derived from aperture photometry while Kent's is derived from an ellipse fitting method. The V surface brightness profile given by Hedge based on photoelectric photometry is plotted also in Figure 7(a), and shows a flatter distribution than ours. Kent (1987) noticed this point earlier and suggested that Hedge's photometry might have been affected by the bright sky at the Mt. Wilson. The $(B - V)$ radial distribution of Hedge is also redder by 0.1 – 0.2 mag than ours. Price (1985) presented surface photometry of NGC 185 based on photoelectric and CCD photometry. The radial distributions of V, $(B - V)$ and $(U - B)$ in her photometry are displayed in Figure 7(a), showing reasonably good agreement with ours.

7.3 Structural Parameters

Structural parameters for NGC 185 have been derived from the surface photometry obtained in this study in combination with the information on the central velocity dispersion given in the literature. The central surface brightness is estimated from the average value for the region of $R < 4$": $\mu_B(0) = 20.54 \pm 0.06$, $\mu_V(0) = 19.73 \pm 0.04$, $\mu_R(0) = 19.18 \pm 0.04$, and $\mu_I(0) = 18.44 \pm 0.04$ mag/arcsec^2. The corresponding absolute magnitudes are -4.22, –4.84, -5.30 and -5.90 mag/arcsec^2, respectively, adopting the distance we measured in this study. The half-brightness radii at B, V, R, and I are measured to be 19".0 (57 pc), 21.8" (65 pc), 23.0" (69 pc), and 28.2" (85 pc), respectively. We take, as a characteristic value, the mean of the values for V and R: 22" $\pm$ 1" (67 $\pm$ 3 pC).

Combining these parameters with the information on the velocity dispersion, we can estimate the mass-to-luminosity ratio. Richstone & Tremaine (1986) showed that the central mass-to-luminosity ratio for most stellar systems with a flat central core, isotropic velocity distribution, and constant mass-to-light ratio can be determined within 2% accuracy using the equation based on the core fitting method,

$$\frac{M}{L} = \frac{90"(0)2}{2\pi G I(0) R_{hb}},$$ (1)

where $\sigma_v(0)$ is a central line-of-sight velocity dispersion and R_{hb} is the half-brightness radius. Expressing the above equation in terms of practical units, we derive

$$\frac{M}{L}\left(\frac{M_\odot}{L_\odot}\right) = 3.33 \times 10^2 \frac{(\sigma_v(0)[km/sec])^2 (a[pc/arcsec])^2}{(R_{hb}[pc]) \, 10^{0.4(M_\odot - \mu_0(0))}},$$ (2)

where a is a geometric scale factor at the distance of the object given in units of pc/arcsec ($= 3.0$ pc/arcsec for NGC 185) and $\mu_0(0)$ is the absolute surface brightness at the center in units of mag/arcsec^2.

Bender *et al.* (1991, called BPN hereafter) concluded that the central velocity dispersion of NGC 185 is $\sigma_v(0) = 22 \pm 4$ km/see, while Held *et al.* (1992) found that the velocity dispersion is constant at 28 ± 8 km/see between 3" and 40" and that it may increase to about twice 'that value in the center. Using equation (2) with the central velocity dispersion given by BPN and adopting $M_{\odot B} = 5.48$ mag and $M_{\odot V} = 4.79$ mag, we obtain the mass-to-luminosity ratio for B and V: $M/L_B = 3.0(M_\odot/L_{\odot B})$ and $M/L_v = 2.9(M_\odot/L_\odot v)$. The total mass of NGC 1.85 can be derived from the central mass-to-luminosity ratio and the total luminosity, if we assume that the mass-to-luminosity is constant. The total B and V magnitudes of NGC 185 are $B_T = 10.13$ mag (Sandage & Tammann 1987) and $VT = 9.05$ mag (Kodaira *et al.* 1990). Adopting the distance we estimated in this study, we obtain $M_B = -14.63$ mag $(L_B = 1..1 \times 10^8 M_{\odot B})$ and $M_V = -15.52$ mag $(L_V = 1.3 \times 10^8 M_\odot v)$. The total mass of the galaxy thus derived is $3.2 \times 10^8 M_\odot$ based on B photometry and $3.8 \times 10^8 M_\odot$ based on V photometry. However, these values are still very uncertain, because the velocity distribution of NGC 185 is known to be anisotropic (BPN and Held *et al.* 1992). (Note that BPN gave $M/L_B = 5 \pm 2(M_\odot/L_{\odot B})$ using the same method. However, the values for the core radius ($\sim 60"$), the surface brightness at the core radius (~ 22.2 mag/arcsec^2), and the distance they used (700 kpc) are much different from those we used in our study.) If

wc use as the central velocity dispersion, σ_v (0) $=$ 28 (or 50) km/see, given by Held *et al.*, *we* obtain the mass-to-luminosity ratio 1.6 (or 5.2) times larger than that based on the central velocity dispersion given by BPN. Note that Held *et al.* obtained the mass-to-luminosity, $M/L_B \approx 3$ following Binney's (1982) formula for an isotropic spherical galaxy with a de Vaucouleurs' profile with some modifications for the effects of oblateness and anisotropy. In summary, all of these estimates suggest that M/L_B for NG C 185 ranges from 3 to 5 under the assumption of a velocity dispersion of 22–28 km/see. However, M/L_B could be as large as 16, if the velocity dispersion is 50 km/see.

8. DISCUSSION

We discuss the properties of stellar populations of NGC 185 in comparison with other Local Group galaxies in this section. We loosely define here " young-age" for $t < 1$ Gyr, "intermediate-age"(for $1 < t < 10$ Gyr, and "old-age" for $t > 10$ Gyr. The old stellar populations have already been discussed in previous sections.

8.1 Young stellar populations

There are several kinds of Population I objects which have been identified in NGC 185: optical dust clouds, HI gas, CO molecular gas, and a possible supernova remnant, in addition to blue stars. HI gas in NGC 185 has been studied by Johnson & Gottesman (1983). Interestingly the center of the HI gas is 30" off from the optical nucleus, and is it not coincident with either of the two dust clouds. Johnson & Gottesman concluded that this offset may be a result of the inhomogeneous physical states of the interstellar medium in NGC 185 (HI, molecular gas, and dust clouds). The integrated flux of the HI gas is 1.511 $\pm$ 0.056 Jy km see-l, corresponding to a total mass of (1.1 $\pm$ 0.1) x $10^5 M_\odot$ under the assumption that the HI gas is optically thin, adjusted to the distance given in this study. Gallagher & Hunter (1981) concluded from a B and I photometric study of the two dust clouds in NGC 185 that they are similar to the molecular clouds in our Galaxy, while the dust clouds in M31 are similar to the HI-dominated diffuse gas. They

suggested that NGC 185 is in an equilibrium state such that the gas shed by old dying stars is recycled to form young stars. CO emission was detected from the center and the dust cloud DC1 located at 21" west of the center by Wiklind & Rydbeck (1986). These authors estimated that the mass of CO clouds is similar to that of the HI gas. Interestingly they found that there are two components with different velocities, one broad component at v_{LSR} = –203 km See–l and one narrow component at v_{LSR} = —292 km see–l. Gallagher *et al.* (1984) measured the intensity of emission lines from the central area of NGC 185 and found that the ratios of emission lines [S11] and [NII] to Hα arc larger than those for typical photo-ionized gas in an HII region. They concluded that the emission gas may be due to a shock-heated supernova remnant, indicating the presence of a Population I component. All of these data indicate that there is a small amount of interstellar material (e. g., 2 x $10^5 M_\odot$ for both HI and CO gas) available for the formation of stars in NGC 185, which are consistent with the presence of a small number of blue stars.

The presence of young stars in NGC 185 has been known since Baade (1951) counted about a dozen B stars with 20 < m_{pg} < 21 mag scattered through this galaxy. Later Hedge (1963, 1973) estimated the total number of Pop I stars to be 17, based on Baade's plate.

A $V - (B - V)$ diagram in Figure 9 shows that there is no conspicuous blue main-sequence typical for late-type galaxies, but a small number ($\sim$ 20) of blue stars scattered around the zero-age main-sequence (ZAMS) line with 20< *V <23* msg. Stars located at R < 10" are plotted by the circled dots, while stars beyond R = 10" are by the dots in Figure 9. Note that the photometry of stars at R < 10" suffers seriously from crowding so that it should be considered cautiously. Figure 2(b) shows that these blue stars arc somewhat concentrated in the central area of NG C 185. The brightest star along the ZAMS line is seen at V = 20.45 mag and $(B - V)$ = –0.14 msg. This star (ID: 5370) is located at $\sim$ 50" south from the center of NG C 185 (see Figure 2(b)). If it is a single

star, it may have a mass of $\sim 20\ M_\odot$, according to the isochrones given by Maeder & Meynet (1991). The second brightest stars are found at $V \approx 21.5$ mag ($M_V \approx -3$ mag) and $(B - V) \approx 0.0$ msg. The presence of these blue stars indicates that NGC 185 might have formed a small number of stars as recently as 20-40 Myr ago.

We also illustrated in Figure 9 the theoretical isochrones for the metallicity Z = 0.001 ([Fe/H] = −0.7) and ages of 200, 300 Myr and 9 Gyr based on the stellar evolutionary models incorporating the convective overshooting atmosphere by Bertelli *et al.* (1990). The isochrones were shifted according to the distance and reddening for NGC 185 determined in this study. The empirical instability strip of the LMC Cepheids is also drawn. Figure 9 shows that the position of the yellow stars fainter than $V \approx 20.6$ mag corresponds to the evolved stage of core He-burning for stars with mass $3 - 4 M_\odot$ (200 -500 Myr) and to the Cepheid instability strip of the LMC. Variability followup is needed to ascertain which stars, if any, are Cepheids, however, because the photometric errors due to severe crowding are large for any individual star.

8.2 *V* Luminosity Function for Blue Stars in NGC 185

The stellar initial mass functions (IMF) of elliptical galaxies are critical for understanding various aspects of elliptical galaxies. However, there has been to date no direct study of the stellar mass functions in elliptical galaxies except for a few studies using starcounts of blue stars in NGC 185 and NGC 205 (e. g., Hedge 1973). The *V* luminosity function of blue stars with colors $(B - V) < 0.6$ mag has been derived in a similar way to that used for other nearby galaxies (Freedman 1985, Hedge *et al.* 1988). It is listed in Table 7 and plotted in Figure 10. The turnover around $V \approx 22.75$ mag is due to the incompleteness in our data, but the luminosity function is probably almost complete up to $V \approx 22.0$ msg. The *V* luminosity function of blue stars in M31-OB80, an OB-association in M31 (Lee 1993) derived from the data obtained in the same observing run as those of NGC 185 is also plotted for comparison. The logarithmic slope of the luminosity function of NGC 185 is very similar to that of M31-OB80. A linear least-squares fit to the

range of $20 < V < 22$ mag formally yields a slope of $-0.54(\pm 0.06)$, which is consistent with other nearby galaxies (Freedman 1985). However, it must be noted that the number of stars available is small. With this caveat in mind, the luminosity function of massive stars in NGC 185 appears to be similar to that of other nearby galaxies.

8.3 Intermediate-age Population

In section 3 we showed that there is a significant excess of bright red stars above the tip of the RGB extending to $I \approx 19$ msg. In order to study comparatively these bright red stars, we have plotted in Figure 11 a schematic locus for the RGB plus AGB of the stellar constellation Shapley 111 in the LMC studied by Reid *et al.* (1987). The tip of the RGB for Shapley 111 is marked by the horizontal solid line connecting the RGB and the AGB. Reid *et al.* (1987) identified the AGB stars in Shapley 111 as intermediate-age populations. Taking into account that the red stars in NG C 185 are slight] y bluer than those of LMC stars because of lower metallicity, these bright red stars are photometrically similar to the AGB stars of LMC Shapley 111. The position of these bright red stars is also consistent with that of carbon star candidates in NGC 205 (open squares) found by Richer *et al.* (1984), as shown in Figure 11. Therefore, most of these bright red stars are likely to be 'an intermediate-age population typified by AGB and carbon stars of $1 - 3M_\odot$ having ages of 1 to several Gyr.

How do the properties of AGB stars in NGC 185 compare with those in M32? Freedman (1992a,b) and Elston & Silva (1992) discussed in detail several possibilities (old long-period variables, old merged binaries, old super-metallicity stars, and an intermediate-age population) to explain bright red giant stars seen in M32, reaching the conclusion that those stars in M32 most likely represent an intermediate-age population. A comparison of the AGB stars in NGC 185 with those in M32 is given in the following. The $I-(V-I)$ diagram of NGC 185 has been converted into the $M_{bol} - (V-I)_0$ diagram using the bolometric corrections given by Da Costa & Armandroff (1990), and has been displayed in Figure 12(a). A $M_{bol} - (V-I)_0$ diagram of a field located 2' south of M32

has been similarly obtained using the photometry given in Freedman (1 989), shown in Figure 12(b) for comparison with NGC 185. Figures 12(a) and (b) show that the M_{bol} magnitudes of these AGB stars range similarly up to -5 mag and that the stars of NGC 185 are bluer than those of M32, again presumably due to their lower metallicity.

8.4 Bolometric Luminosity Function for the AGB Stars in NGC 185

Following the method given by Reid & Mould (1984), we have derived the bolometric luminosity function of the AGB stars in NGC 185 by counting stars with $(V - I)_0 >$ 1.48 msg. The luminosity functions for the AGB stars as well as for both the RGB and AGB stars are listed in Table 8 and plotted in Figure 13. Using the same method, we also constructed the bolometric luminosity functions for the AGB stars in M32 from the *VI* photometry given in Freedman (1989). The bolometric luminosity function for M32 is drawn in Figure'13 in comparison with that for NGC 185. We adopted a distance modulus to M32, $(m - M)_0$ = 24.38 msg. The luminosity function for M32 was shifted vertically to match the NGC 185 luminosity function at M_{bol} = —4.0 mag in Figure 13. Figure 13 shows the following features: (1) The luminosity function for NGC 185 extends up to $M_{bol} \approx$ –5.0 msg. There are a few stars brighter than M_{bol} = –5.0 msg. M_{bol} = —5.0 mag of the AGB stars corresponds to an age of $\sim 3 \pm 3$ Gyr and a stellar mass of $\sim 1.4\ M_\odot$, according to Iben & Renzini (1983, their Figure 7) and Reid *et al.* (1990, their Figure 1); and (2) The luminosity function for NGC 185 is very similar to that for M32 in general. Freedman (1992) noted that some very red bright stars which are visible on near-IR images are not always detected at optical *I*-band images. Therefore the very upper end of the luminosity functions we derived in this study is not complete. It is very difficult to combine reliably the AGB luminosity functions derived from the optical photometry and those from the near-IR photometry at this moment. However, it will be easier when the near-IR photometry of the red giant stars in these galaxies reaches 1-2 mag deeper than those presently available.

9. SUMMARY AND CONCLUSIONS

The primary results from this $B VRI$ study of $\sim$ 5,300 stars in NGC 185 are summarized as follows:

1. The color-magnitude diagrams show three distinct stellar populations: (1) a dominant red giant branch population, (2) asymptotic giant branch stars located above the tip of the red giant branch stars and (3) a small number of young stars having blue to yellow colors.

2. The foreground reddening has been estimated to be $E(B - V) = 0.19 + 0.03$ mag using the $(B-V) - (V-I)$ diagram for the bright foreground stars with good photometry.

3. The tip of the red giant branch has been detected at $I = 20.30 \pm 0.20$ mag and $(V-I) = 1.95 \pm 0.05$ msg. The distance has been estimated to be $(m-M)_0 = 23.96 \pm 0.21$ mag ($= 620 \pm 60$ kpc) from the I magnitude of the tip of the red giant branch.

4. The metallicity of giant stars has been estimated using the $(V - I)$ color at $M_I = -3.5$ mag, $(V - I)_{-3.5,0} = 1.494 \pm 0.036$ mag, to be [Fe/H] $= -1.23 \pm 0.16$ dex and the color dispersion of A $(V - I)_{-3.5} = 0.12$ mag yields a metallicity dispersion of $-1.6 <$ [Fe/H] < -0.9 dex.

5. Surface photometry of the central area $(R < 50")$ of NGC 185 has been presented, showing that colors get rapidly bluer inside $R \approx 10"$. Structural parameters indicate that the mass-to-luminosity ratio M/L_B ranges from 3 to 5.

6. A V luminosity function for the blue stars has been derived. The slope of the luminosity function is found to be very similar to that for other nearby, but late-type, galaxies.

7. The bolometric luminosity function of the AGB stars in NGC 185 extends to $M_{bol} \approx -5.0$ mag, corresponding to an age of $\sim 3 \pm 3$ Gyr and a stellar mass of $\sim 1.4 M_\odot$. The bolometric luminosity function of the AGB stars in NGC 185 is very similar to that of M32.

REFERENCES

Baade, W. 1944, ApJ, 100, 147

Baade, W. 1951, *Publ. Univ. Mich. Ohs.,* 10, *7*

Barsony, M. A. 1989, Ph.D. Thesis (Caltech)

Bender, R., Paquet, A., & Nieto, J.-L. 1991, A&A, 246,349 (BPN)

Bertelli, G., Betto, R., Bressan, A., Chiosi, C., Nasi, E., & Vallenari, A. 1990, A&AS, 85, 845

Binncy, J. 1982, ARA&A, 20, 399

Binney, J., & Tremaine, S. 1987, Galactic *Dynamics,* (Princeton: Princeton University Press), Chap. 4.

Burstein, D., & Heiles, C. 1982, AJ, 87, 1165

Cardelli, J. A., Clayton, G. C., & Mathis, J. S. 1989, ApJ, 345, 245

Ciadullo, Jacoby, G. H., Ford, H. C., & Neill, J. D. 1989, ApJ, 339, 53

Cousins, A. W. J. 1978, MNASSA, 37, 62

Da Costa, G. S., & Mould, J. R. 1988, ApJ, 334, 159

Da Costa, G. S., & Armandroff, T. E. 1990, AJ, 100, 162

Djorgovski, S. 1988, in IAU Symposium No. 126, *The Harlow-Shapley Symposium on Globular Cluster Systems in Galaxies,* eds. J. E. Grindly & A. G. Davis

Philip, (Dordrecht: Reidel), 333

Dressel, L. L., & Condon, J. J. 1976, ApJS, 31, 187

Elston, R., & Silva, D. R. 1992, AJ, 104, 1360

Ford, H. C., Jacoby, G., & Jenner, I), C. 1977, ApJ, 213, 18

Freedman, W. L. 1985, ApJ, 299, 74

Freedman, W. L, 1989, AJ, 98, 1285

Freedman, W. L. 1992a, in IAU Symp. No. 149, *The Stellar Populations of Galaxies,* eds. B. Barbuy & A. Renzini, (Dordrecht: Kluwer), 169

Freedman, W. L. 1992b, AJ, 104, 1349

Gallagher HI, J. S., Hunter, D. A. 1981, AJ, 86, 1312

Gallagher III, J. S., Hunter, D. A., & Mould, J. R. 1984, ApJ, 281, 63

Harris, W. E. 1991, ARA&A, 29, 543

Held, E. V., de Zeeuw, T., Mould, J., & Picard, A. 1992, AJ, 103, 851

Hedge, P. W. 1963, AJ, 68, 692

Hedge, P. W. 1973, ApJ, 182, 671

Hedge, P. W. 1974, PASP, 86, 289

Hedge, P. W. 1989, ARA&A, 27, 139

Hodge, P. W., Lee, M. G., & Mateo, M. L. 1988, PASP, 324, 172

Johnson, D. W., & Gottesman, S. T. 1983, ApJ, 275, 549

Kent, S. M. 1987, AJ, 94, 306

Kodaira, K., Okamura, S., & Ichikawa, S. 1990, Photometric *Atlas of Northern Bright Galaxies,* (Tokyo: Univ. of Tokyo Press)

Lee, M. G. 1990, Ph. D. Thesis (University of Washington)

Lee, M. G. 1993, in preparation

Lee, M. G., Freedman, W. L., & Madore, B. F. 1992a, in IAU Symp. No. 149, *The Stellar Populations of Galaxies,* eds. B. Barbuy & A. Renzini, (Dordrecht: Kluwer), 444

Lee, M. G., Freedman, W. L., & Madore, B. F. 1992b, in IAU Symp. No. 149, *The Stellar Populations of Galaxies,* eds. B. Barbuy & A. Renzini, (Dordrecht: Kluwer), 445

Lee, M. G., Freedman, W. L., & Madore, B. F. 1993a, submitted to ApJ

Lee, M. G., Freedman, W. L., & Madore, B. F. 1993b, in preparation

Lee, Y.-W. 1992, *Mere. Sot. Astro. Italiana, 63, 331*

Maeder, A., & Meynet, G. 1991, A&AS, 89,451

Mateo, M. L., Saha, A., & Schechter, P. L. 1990, DoPHOT User's Manual

Madore, B. F., & Freedman, W. I.. 1991, PASP, 103, 933

Mould, J. R., Kristian, J. 1986, ApJ, 305, 591

Price, J. S. 1985, ApJ, 297, 652

Ratnatunga, K. U., & Bahcall, J. N. 1985, ApJS, 59, 63

Reid, N., & Mould, J. 1984, ApJ, 284, 98

Reid, N., Mould, J., & Thompson, I. 1987, ApJ, 323, 433

Reid, N., Tinncy, C., & Mould, J. 1990, ApJ, 348, 98

Richstone, D. O., & Tremaine, S. 1986, AJ, 92, 72

Saha, A., & Hoessel, J. G. 1990, AJ, 99, 97

Sandage, A. R., & Tammann, G. A. 1987, *A Revised Shapley-Ames Catalog of Bright Galaxies, (Washington,* D. C.: Carnegie Institution)

van den Bergh, S. 1975, ARA&A, 13, 217

Wiklind, T., & Rydbeck, G. 1986, A&A, 164, L22

Wilson, C. D., Freedman, W. L., & Madore, B. F. 1990, AJ, 99, 149

TABLE 1. Basic information for NGC 185.

Parameter	Information	Reference
α_{1950}	$00^h\,36^m\,128.0$	Dressel & Condon (1976)
δ_{1950}	+48° 03'50"	Dressel & Condon (1976)
l, b	120.80, –14.48 deg	Sandage & Tammann (1987)
v_r , v_{rot}	–202 ± 3,–1.2A 1.1 km/s	Bender et al. (1991)
$\sigma_v\ (R = 0)$,σ_v (mean)	$22 \pm 4, 23 \pm 5$ km/s	Bender et al. (1991)
Apparent size	14'.5 X 12'.3	Baade (1944)
$(m - M)$.	23.96 ± 0.21 (=620 kpc)	This study
Half-brightness radius, R_{hb}	22" ±1"(=64 ± 3 pC)	This study
$\mu_B(R = 0)$	20.54 mag/arcsec^2	This study
$\mu_V(R = 0)$	19.76 mag/arcsec^2	This study
B_T, M_B	10.13, –14.63 mag	Sandage & Tammann (1987)
V_T, M_V	9.05, –15.52 mag	Kodaira et al. (1990)
Morphological type	dE3pec	Sandage & Tammann (1987)
$E(B - V)$ (foreground)	0.19 ± 0.03 mag	This study
M_{HI}^a	1.1 x $10^5 M_\odot$	Johnson & Gottesman (1983)
M_{CO}^a	$\sim 10^5 M_\odot$	Wiklind & Rydbeck (1986)
No. of globular clusters	6	Ford et al. (1977)
[Fe/H] of globular clusters	–1.65 ± 0.25 dex	Da Costa& Mould (1988)
[Fe/H] of the RGB	–1.29 ± 0.08 dex	This study
No. of RR Lyraes	151	Saha & Hoessel (1990)
[Fe/H] of RR Lyraes	–1.0 to -2.0 dex	Saha & Hoessel (1990)

[a] Corrected for the distance adopted in this paper.

TABLE 2. Journal ofobservations for NGC 185.

Filters	T_{exp}	Air Mass	FWHM	U.T.
B	530 sec	1.16	0".75	1987 Sep 2210:10
v	400 Sec	1.15	0".70	1987 Sep 22 10:20
R	100 sec	1.16	0".62	1987 Sep 2210:03
I	200 sec	1.16	0".61	1987 Sep 22 10:06

TABLE 4a. Mean photometric errors versus V for NGC 185.

v	σ_V	$\sigma_{(B-V)}$	$\sigma_{(V-I)}$
20.25	0.02	0.03	0.03
20.75	0.03	0.04	0.05
21.25	0.04	0.08	0.06
21.75	0.06	0.11	0.08
22.25	0.08	0.15	0.11
22.75	0.11	0.20	0.15
23.25	0.16	0.25	0.20

TABLE 4b. Mean photometric errors versus I for NGC 185.

I	σ_I	$\sigma_{(B-V)}$	‘(V-I)
18.75	0.02	0.07	0.04
19.25	0.03	0.08	0.06
19.75	0.04	0.12	0.08
20.25	0.06	0.13	0.10
20.75	0.08	0.15	0.13
21.25	0 . 1 2	0.18	0.17
21.75	0.18	0.20	0.22

TABLE 5. Expected number of Galactic foreground stars for NGC 185".

V	$(B - V) < 0.8$	$0.8 < (B - V) < 1.3$	$(B - V) > 1.3$	Total
13-15	0.54	0.34	0.04	0.92
15-17	1.15	1.91	0.18	3.21
17–19	0.77	5.89	1.53	8.42
19-21	0.40	4.97	7.65	13.01
21-23	0.53	1.30	20.66	22.19

[a] Numbers of stars expected in the area of the CCD field (7.65 arcmin^2).

TABLE 6. V and I luminosity functions of the red giant stars in NGC 185.

v	N(ALL)	N($R > 40$")	I	N(ALL)	N($R > 40$")
20.55	3	3	18.95	1	1
20.65	0	0	19.05	3	1
20.75	1	0	19.15	2	2
20.85	1	0	19.25	10	5
20.95	5	0	19.35	13	10
21.05	5	3	19.45	23	9
21.15	3	3	19.55	32	14
21.25	7	3	19.65	52	27
21.35	14	7	19.75	41	21
21.45	22	13	19.85	60	35
21.55	35	15	19.95	92	51
21.65	54	20	20.05	121	65
21.75	85	46	20.15	131	85
21.85	91	48	20.25	200	126
21.95	193	103	20.35	230	155
22.05	209	127	20.45	290	204
22.15	309	203	20.55	318	225
22.25	332	232	20.65	362	248
22.35	380	279	20.75	376	289
22.45	449	331	20.85	398	290
22.55	523	390	20.95	366	286
22.65	498	392	21.05	350	237
22.75	454	347	21.15	309	235
22.85	381	284	21.25	272	205
22.95	281	217	21.35	239	185
23.05	238	167	21.45	189	142
23.15	141	108	21.55	142	102
23.25	96	77	21.65	126	91
23.35	52	39	21.75	79	63
23.45	28	20	21.85	38	24

TABLE 7. *V* luminosity function of blue stars with $(B - V)$ <0.6 mag in NGC 185.

V	M_v	N(V)	N(< V)
19.5-20.0	*−5.01 − −4.51*	*1*	1
20.0-20.5	−4.51 − −4.01	1	2
20.5−21.0	−4.01 − −3.51	4	6
21.0-21.5	−3.51 − --3.01	6	12
21.5−22.0	−3.01 − −2.51	10	22
22.0-22.5	−2.51 − −2.01	18	40
22.5−23.0	−2.01 − −1.51	25	65
23.0-23.5	−1.51 − −1.01	12	77

TABLE 8. M_{bol} luminosity function of the red giant stars in NGC 185.

M_{bol}	N(RGB+AGB)	N(AGB)
−5.35	1	0
−5.25	1	1
−5.15	o	0
−5.05	1	1
--4.95	2	2
−4.85	4	2
−4.75	6	6
-4.65	13	4
−4.55	12	12
−4.45	22	10
−4.35	27	24
-4.25	38	21
−4.15	50	42
−4.05	63	42
−3.95	64	49
−3.85	94	53
-3.75	104	74
−3.65	141	71
−3.55	179	85
−3.45	243	98
−3.35	265	124
−3.25	281	128
-3.15	277	122
−3.05	329	74
−2.95	350	75
-2.85	341	56
−2.75	353	53
−2.65	284	28
−2.55	291	12
−2.45	246	11
−2.35	196	7

I? IGURE CAPTIONS

FIG. 1. — CCD images of NGC 185. North is at the top and East is to the left. The scale is 0".205 /pixel and the size of the field is 640 x 1024 pixels (131" x 210"). (a) Reproduction of a B CCD image of NGC 185. (b) Reproduction of a V CCD image of NGC 185. (c) Reproduction of an I CCD image of NGC 185.

FIG. 2. — Finding charts for the measured stars in NGC 185. North is at the top and East is to the left, (a) A finding chart for all the measured stars with $V < 23$ mag in NGC 185. Stars with $V < 21$ mag are labeled. (b) A finding chart for blue stars with $(B - V) < 0.6$ msg. Stars with $V < 21$ mag are labeled. Note that the blue stars are concentrated in the central area. (c) A finding chart for bright red giant stars with $17.5 < 1 < 20$ mag and $(V - I) > 1.4$ msg. Stars with $I < 19$ mag are labeled.

FIG. 3. — Color-magnitude diagrams for $\sim 5,300$ stars in NGC 185. (a) $V - (B - V)$ diagram. (b) $V - (V - I)$ diagram. (c) $I - (R - I)$ diagram. (d) $I - (V - I)$ diagram.

FIG. 4. — $(B - V) - (V - I)$ diagram for stars in NGC 185 with $V < 20$ mag and internal photometric errors smaller than 0.05 msg. The solid line depicts a reddening direction. Short dashed and long dashed lines represent the intrinsic relations for dwarfs and giants, respectively, which are shifted according to the reddening of $E(B - V) = 0.19$ mag along the reddening line.

FIG. 5. — $I - (V - I)$ diagram for stars located at $R > 40$". Mean photometric errors are shown by error bars to the left. The solid curved lines show from the left to the right the loci for the giant branches of Galactic globular clusters, M15, M2, NGC 1851, and 47 Tut, the metallicities of which are, respectively, [Fe/H] = −2.17, −1.58, −1.29, and −0.71 dex.

FIG. 6. — I luminosity functions (a) for the red giant stars located at R > 40" and (b) for all the measured stars in NGC 185. The solid lines represent the I luminosity functions and the dotted lines the convolution of the luminosity functions with the edge-detector described in the text. The position of the tip of the red giant branch is marked as TRGB.

FIG. 7. — Surface photometry of the central area within R= 50" of NGC 185. (a) Upper panel: Surface brightness profiles versus effective radius. Gunn r photometry of Kent (1987) is transformed to Cousins R magnitude by using $R = r - 0.31$, and is represented by a dashed line. V photometry of Hedge (1963) is shown by a dotted line. Lower panel: Differential colors versus effective radius. $(B - V)$ photometry from Hedge (1963) are shown by the dotted line. (b) Upper panel: Integrated magnitudes versus R_{out}(=outer radius of the given aperture). V photometry of Price (1985) is shown by a dotted line. Lower panel: integrated colors versus R_{out}. $(U - B)$ and $(B - V)$ colors of Price (1985) are displayed by dotted lines and $(13 - V)$ photometry of Hedge (1963) is plotted by a dashed line.

FIG. 8. — Radial variation of magnitudes and colors. Colors are plotted for stars with $V < 22$ mag' to avoid any selection effect due to incompleteness. Note that there is an excess of blue stars in the central area, while the color gradient is almost negligible in the outer area.

FIG. 9. — $V - (B - V)$ diagram of all the measured stars in NGC 185. The stars located within 10" are marked by circled dots. The mean errors for various magnitudes are shown by error bars to the right. and $M = 7,6,5,4, 3M_{\odot}$ Curved dashed and solid lines show the theoretical isochrones for metallicity Z = 0.001 ([Fe/H] = -0.7) and ages, 200, 300 Myr and 9 Gyr based on the stellar evolutionary models incorporating convective-overshooting atmosphere by Bertelli et al. (1990). The dotted line represent

the ZAMS with solar metallicity. Two slanted parallel lines represent the position of the Cepheid instability strip based on observations in the LMC.

FIG. 10. — V luminosity functions of blue stars with $(B - V) < 0.6$ mag of NGC 185 (filled circles with the solid line). The luminosity function of blue stars in OB-80, an 013 association of M31 (open circles with the dashed line) is shown for comparison. The dotted line represents a linear least-square fit line with a logarithmic slope of 0.54(+0.06).

FIG. 11. — $I - (V - I)$ diagram for NGC 185 for comparison with LMC and NGC 205. Schematic loci for the red giant branch plus asymptotic giant branch for the northern field in the LMC are shown by solid lines and several known carbon star candidates in NGC 205 arc plotted by open squares.

FIG. 12. — (a) $M_{bol} - (V - I)_0$ diagram for the stars in NGC 185. (b) $M_{bol} - (V - I)_0$ diagram for the stars in M32. Note that the red stars in NGC 185 are bluer than those of M32.

FIG. 13. — The bolometric luminosity function of the asymptotic giant branch stars in NGC 185 (filled circles) compared with M32 (crosses). The luminosity functions are normalized at the magnitude $M_{bol} = -4$ msg. Note the remarkable similarity between NGC 185 and M32.

TABLE 3a. *BVRI* CCD photometry of stars with $v < 22$ mag in NGC 185

Star	X	Y	V	(B-V)	(V-R)	(V-I)	I	Star	X	Y	V	(B-V)	(V-R)	(V-I)	I
27	558.3	12.3	20.17	0.96	0.42	1.00	19.17	986	429.5	263.2	21.43	1.59	0.92	1.78	19.66
113	237.4	55.3	21.47	0.87	0.49	1.25	20.22	988	572.3	263.5	21.81	1.36	0.61	1.52	20.29
251	604.8	108.4	18.15	0.76	0.27	0.81	17.33	1019	318.2	267.0	21.86	2.14	0.97	2.13	19.73
277	211.1	115.9	20.05	0.83	0.34	0.89	19.16	1041	166.8	270.5	21.48	1.85	0.75	1.30	20.19
280	313.1	116.4	21.39	1.71	0.49	1.22	20.18	1045	394.5	270.8	21.40	1.89	1.02	2.09	19.32
305	546.8	122.1	21.39	1.64	0.72	1.70	19.68	1071	153.2	274.3	21.61	1.54	0.62	1.54	20.07
315	457.3	126.6	21.27	0.34	0.03	0.39	20.88	1072	180.6	274.5	21.59	1.61	0.57	1.49	20.11
477	511.2	168.7	21.81	1.51	0.89	1.89	19.92	1079	445.6	275.5	21.70	1.26	0.70	1.43	20.27
548	260.7	185.9	21.53	1.39	0.65	1.46	20.07	1087	386.1	276.1	21.91	1.77	0.74	1.75	20.17
563	565.7	189.8	21.61	1.27	0.53	1.39	20.23	1094	466.9	277.3	21.25	1.55	1.00	2.15	19.11
576	417.2	192.7	21.34	1.99	0.89	1.96	19.39	1102	503.9	278.3	21.75	1.64	0.77	1.57	20.19
597	335.6	196.1	21.86	1.46	0.76	1.63	20.23	1115	620.7	279.5	20.28	0.85	0.40	1.16	19.12
628	387.3	202.3	20.62	0.44	0.26	0.45	20.18	1160	500.1	285.8	21.81	1.57	0.75	2.09	19.72
673	542.6	211.5	21.77	1.60	0.32	1.07	20.70	1171	511.3	286.6	21.87	1.39	0.87	1.47	20.41
681	345.8	212.4	21.68	1.85	0.85	2.08	19.60	1208	588.0	291.6	21.73	1.74	0.75	2.31	19.43
712	546.5	218.8	17.10	0.94	0.46	1.05	16.06	1220	427.8	293.5	21.08	1.02	0.56	1.26	19.82
732	521.3	223.3	21.73	1.78	0.84	1.99	19.74	1223	629.8	293.9	21.96	1.71	0.79	1.75	20.22
763	184.5	229.1	21.96	1.35	0.77	1.35	20.62	1235	244.5	295.0	21.91	1.81	0.74	1.75	20.17
766	283.9	229.6	21.39	1.14	0.86	1.65	19.74	1236	254.8	295.1	20.57	1.08	0.53	1.09	19.49
813	302.5	237.4	21.97	1.51	0.69	1.49	20.49	1252	357.5	296.6	21.66	0.93	1.01	2.06	19.60
818	561.3	237.9	21.80	1.82	0.67	1.71	20.10	1265	298.2	298.3	21.12	1.53	0.93	1.84	19.28
835	538.8	241.7	21.67	0.96	1.11	2.08	19.59	1272	375.2	299.0	21.89	1.71	0.76	1.97	19.92
862	521.7	245.6	21.98	1.17	0.50	1.27	20.72	1301	214.3	302.7	21.94	1.82	0.68	1.07	20.88
865	400.1	245.8	21.84	1.29	0.50	1.69	20.15	1369	119.3	310.0	20.53	1.81	0.86	2.32	18.21
882	208.8	248.2	21.84	1.70,	0.75	1.55	20.30	1377	605.3	310.5	21.97	1.53	0.70	1.86	20.11
899	355.2	251.0	21.79	1.45 '	0.65	1.33	20.46	1382	308.5	311.0	21.59	1.11	0.91	1.55	20.03
901	304.3	251.0	21.95	1.46	0.72	1.49	20.46	1390	185.5	311.7	21.87	1.85	0.82	1.73	20.15
909	544.1	252.0	15.90	1.09	0.59	1.18	14.73	1391	388.3	311.9	21.69	1.37	0.62	1.08	20.62
948	548.8	258.8	19.02	1.05	0.46	1.10	17.92	1428	219.0	315.3	21.24	0.43	0.18	0.40	20.84
976	358.8	261.8	21.97	1.63	0.66	1.76	20.21	1458	368.2	318.5	21.33	1.49	0.90	1.81	19.51
1461	631.1	318.6	19.54	1.37	0.69	1.51	18.03	2024	208.7	383.4	20.99	1.45	0.70	1.51	19.49
1487	143.1	322.3	21.71	1.26	0,63	1.18	20.53	2081	334.0	390.9	21.77	0.96	0.62	1.55	20.23
1513	507.2	325.1	21.91	1.79	0.33	1.34	20.58	2091	559.2	391.7	21.72	1.64	0.75	1.87	19.86
1514	522.2	325.2	21.99	1.98	0.44	1.51	20.49	2103	299.2	393.5	21.54	1.70	0.94	2.28	19.26
1539	527.7	329.1	21.91	1.30	0.53	1.65	20.26	2123	317.2	395.9	21.76	1.41	0.67	1.40	20.36
1541	516.8	329.2	21.97	1.72	0.78	1.76	20.21	2146	497.4	398.0	21.55	1.53	0.74	1.96	19.59
1542	248.0	329.3	21.06	1.24	0.63	1.21	19.86	2239	93.7	408.8	19.07	1.48	0.78	1.68	17.39
1700	447.3	347.0	21.98	1.39	0.48	1.62	20.37	2241	441.2	409.0	21.78	1.90	0.48	1.52	20.27
1714	88.3	349.2	20.18	1.74	0.88	2.10	18.08	2244	413.1	409.2	20.99	0.59	0.35	1.16	19.83
1729	142.0	350.8	17.53	0.77	0.37	0.83	16.70	2267	347.4	411.4	21.95	2.11	1.08	2.42	19.53
1745	599.5	352.1	21.92	1.50	0.79	1.69	20.24	2303	459.5	417.3	21.80	1.48	0.92	2.09	19.71
1750	247.6	352.5	21.30	0.58	0.34	0.99	20.31	2330	542.6	420.8	21.99	1.40	0.92	1.63	20.37
1768	438,9	354,8	21.86	1.70	0.06	1.60	20.27	2335	256.0	421.4	18.58	0.69	0.27	0.79	17.80
1777	202.1	355.8	21.72	1.47	0.70	1.71	20.01	2340	399.1	422.0	21.63	1.09	0.54	1.58	20.06
1782	434.5	356.8	21.44	1.47	0.77	2.01	19.43	2345	307.9	422.2	21.70	1.86	0.91	1.94	19.76
1796	424.1	358.3	21.94	1.60	0.51	1.27	20.67	2355	233.1	423.6	21.96	1.85	0.67	1.93	20.04
1812	284.5	359.4	21.62	1.43	0.51	1.41	20.22	2363	406.2	424.1	21.97	0.85	0.46	1.13	20.84
1813	374.0	359.4	21.85	1.42	0.59	1.41	20.44	2364	421.4	424.2	21.70	1.89	0.90	1.90	19.81
1819	363.6	360.2	21.73	1.50	0.73	1.64	20.09	2386	225.9	427.5	21.76	1.39	0.67	1.56	20.21
1839	318.8	362.8	20.88	0.49	0.09	0.86	20.02	2393	449.6	428.3	21.61	1.56	0.62	1.79	19.82
1857	107.7	364.3	21.99	1.76	0.60	1.45	20.54	2398	38.7	428.9	21.75	1.67	0.63	1.11	20.64
1867	264.3	365.7	21.96	1,58	0.73	1.76	20.20	2410	158.9	430.4	21.76	2.55	0.96	2.09	19.68
1884	222.2	367.6	21.94	1.72	0.68	1.41	20.53	2416	512.7	430.8	21.91	1.20	0.86	2.11	19.80
1903	290.2	369.7	21.58	2.13	0.97	2.34	19.24	2419	120.3	431.0	17.26	0.83	0.38	0.92	16.34
1911	466.7	370.5	21.62	1.93	0.81	1.90	19.72	2430	564.6	432.1	21.56	1.60	0.60	1.47	20.09
1917	269.2	371.1	21.61	1.21	0.67	1.58	20.04	2441	396.7	433.2	16.03	0.77	0.39	0.85	15.18
1929	617.7	372.4	21.78	1.55	0.48	1.09	20.70	2485	123.8	438.4	21.75	1.37	0.36	1.49	20.26
1936	336.7	373.0	21.71	1.32	0.81	1.78	19.93	2495	23.9	439.2	21.67	1.84	0.90	2.10	19.57
1957	307.2	375.1	21.28	1.67	0.80	1.84	19.44	2521	519.5	441.9	21.80	1.78	0.43	1.58	20.23
1986	308.0	378.1	21.50	1.76	0.59	1.67	19.83	2523	416.9	442.2	21.53	1.28	0.64	1.58	19.95

Star	x	Y	v	(B-V)	(V-R)	(V-I)	I	Star	x	Y	v	(B-v)	(V-R)	(V-I)	I
2531	373.3	443.2	21.75	1.20	0.45	1.32	20.43	2930	337.4	484.3	21.66	1.10	0.28	1.73	19.93
2532	467.9	443.3	21.92	1.31	0.79	1.94	19.98	2933	364,6	484.6	20.92	0.74	0.23	1.37	19.55
2551	479.3	445.1	21.77	1.71	0.81	1.79	19.99	2934	469.1	484.6	21.34	1.70	0.82	1.73	19.62
2564	253.4	446.7	21.96	1.49	0.82	1.82	20.14	2944	534.9	485.5	21.88	1.33	0.69	1.56	20.33
2573	633.5	447.3	21.43	1.89	0.89	1.53	19.91	2974	347.3	488.4	21.65	0.71	0.79	1.42	20.23
2587	630.1	448.7	21.77	1.36	1.08	1.97	19.80	2980	277.9	488.7	21.35	2.52	0,80	1.76	19.61
2598	140.0	449.8	17.96	0.74	0.32	0.84	17.12	3003	350.5	491.2	21.96	0.61	0,83	1.91	20.05
2607	381.6	450.3	21.83	1.05	0.52	1.70	20.13	3047	352.4	495.1	21.95	1.34	0.77	1.49	20.46
2609	447.4	450.7	21.92	1.60	0.68	1.60	20.33	3082	349.5	499.1	21.70	1.31	0.63	1.39	20.32
2649	364.8	455.2	21.84	1.05	0.75	2.34	19.50	3085	444.4	499.5	21.75	1.39	0.73	1.51	20.25
2662	211.9	456.4	21.94	1.34	0.68	1.52	20.42	3088	75.7	499.8	21.78	1.41	0.68	1.49	20.30
2668	417.8	457.0	21.49	2.82	0.82	1.74	19.76	3095	297.9	500.7	21.07	0.13	0.06	0.48	20.60
2678	414.8	458.0	21.93	2.26	0.83	1.49	20.45	3108	70.1	501.8	21.88	1.61	0.33	1.28	20.60
2692	293.3	459.4	21.59	1.03	0.54	1.75	19.84	3116	428.8	502.4	19.75	0.41	0.09	0.43	19.32
2713	505.1	461.6	21.74	1.47	0.62	1.16	20.58	3135	449.6	504.1	21.63	1.70	0.92	2,08	19.55
2733	393.8	464.4	21.96	0.83	0.62	2.03	19.94	3149	121.8	505.4	21.48	1.83	0.77	2.08	19.40
2753	185.2	466.7	21.79	1.61	0.67	1.83	19.96	3161	310.6	506.4	21.83	1.56	0.68	1.72	20.11
2755	459.7	466.9	21.75	1.26	0.86	2.11	19.64	3174	486.3	507.5	21.74	1.54	0.87	1.87	19.88
2799	524.5	471.8	21.88	1.28	0.80	1.24	20.64	3179	226.7	507.8	21.61	1.64	0.74	1.93	19.68
2802	519.1	472.3	21.80	1.80	0.70	2.15	19.66	3186	263.0	508.2	21.88	1.46	0.86	1.80	20.09
2806	261.3	472.6	18.63	0.94	0.41	1.01	17.61	3187	355.6	508.4	21.54	-0.24	0.40	1.98	19.55
2834	172.5	474.4	21.64	1.42	0.52	0.99	20.66	3211	372.5	510.5	21.95	0.48	0.08	2.48	19.47
2840	489.5	474.8	21.90	1.58	0.66	1.76	20.14	3212	166.2	510.7	21.92	1.35	0.50	1.36	20.57
2859	253.2	477.0	21.37	2.08	0.71	2.13	19.24	3219	391.0	511.3	21.84	0.36	0.00	0.69	21.16
2876	358.6	478.5	21.52	0.82	0.49	1.18	20.34	3246	369.9	513.4	21.93	0.88	0.64	1.99	19.94
2881	623.6	479.3	21.89	1.63	0.94	2.10	19.79	3247	608.3	513.4	21.83	1.74	0.64	1.62	20.21
2886	212.9	479.5	21,84	2.00	1.01	2.30	19.54	3250	182.5	513.8	21.53	1.39	0.63	1.53	20.00
2893	365.2	480.1	21.28	0.20	-0.07	0.12	21.16	3256	411.9	514.0	21.68	1.69	0.70	1.54	20.14
2911	249.9	482.5	21.98	1.50	0.59	1.84	20.15	3261	401.5	514.3	21.92	0.95	0.38	1.38	20.53
2924	361.2	483.2	22.00	1.23	0.90	1.60	20.40	3266	247.0	514.6	21.36	1.60	0.69	1.09	20.28
3269	395.0	514.8	21.60	1.04	0.47	1.49	20.11	3697	292.1	556.0	21.91	1.06	0.35	1.75	20.17
3280	504.3	516.0	21.83	1.43	0.65	1.32	20.52	3704	498.6	556.4	21.90	1.67	0.24	1.82	20.08
3286	386.4	516.6	21.76	1.69	0.41	1.31	20.45	3706	564.5	556.5	21.93	1.47	0.93	1.53	20.41
3294	415.8	517.6	21.92	1.63	0.41	1.42	20.50	3738	74.3	559.5	21.95	1.64	0.56	1.36	20.60
3312	308.2	518.9	21.99	1.10	0.62	1.30	20.69	3747	336.5	560.8	21.96	0.99	0.32	1.25	20.71
3318	314.0	519.1	21.87	1.24	0.58	1.76	20.11	3749	179.3	560.8	21.08	1.68	0.86	1.61	19.48
3330	333.4	520.1	21,71	0.77	0.55	0.95	20.75	3780	450.0	564.9	21.76	1.70	0.98	1.81	19.95
3349	306.0	521.8	21.49	1.69	1.01	2.12	19.37	3785	85.3	565.5	21.94	1.95	0.71	1,49	20.46
3363	629.8	523.1	21.53	1.19	0.45	1.57	19.96	3790	325.1	566.0	21.80	1.87	0.77	1.87	19.94
3367	390.7	523.2	20.95	0.71	0.56	1.63	19.32	3799	593.1	566.7	21.96	1.55	0.56	1.41	20.56
3379	518.0	523.8	21.93	1.30	0.95	1.40	20.53	3802	528.3	567.1	20.99	0.82	0.57	1.57	19.42
3400	174.9	526.2	21.97	1.50	0.85	2.19	19.78	3808	429.1	567.3	21.53	1.34	0.68	1.38	20.16
3418	242.2	527.7	21.41	1.38	0.70	1.80	19.61	3825	352.1	569.8	21.71	1.14	0.57	1.60	20.11
3433	321.5	528.8	21.65	1.18	0.79	2.11	19.55	3834	519.6	570.5	21.92	1.62	0.57	1.65	20.27
3445	181.4	529.8	21.80	1.77	0.74	1.52	20.28	3835	447.4	570.5	21.91	1.68	0.60	1.64	20.28
3464	481.9	531.4	18.08	1.61	0.85	1.99	16.09	3844	556.3	571.7	21.84	1.91	0,83	2.00	19.84
3467	419.8	531.7	21.72	1.13	0.79	1.62	20.10	3846	423.7	571.9	21.91	1.36	0.66	1.30	20.61
3469	369.7	532.0	21.36	1.14	0.73	1.59	19.77	3854	444.6	573.1	21.49	1.97	1.06	2.11	19.39
3471	19.0	532.1	21.52	1.85	0.95	2.06	19.47	3877	312.5	576.2	21.79	1.60	0.53	1.58	20.22
3479	325.2	532.5	21.78	1.22	0.64	1.65	20.13	3918	376.1	580.0	21.63	1.35	0.85	1.86	19.77
3486	599.2	533,1	20.46	1.14	0.52	1.34	19.12	3936	235.7	582.1	21.83	1.28	0.60	1.52	20.31
3498	320.4	534.1	21.97	1.61	0.70	1.84	20.13	3950	111.0	584.4	21.86	1.31	0.74	1.57	20.30
3514	249.2	535.2	21.66	1.36	0.65	1.83	19.84	3955	56.3	585.0	21.83	1.30	0.63	1.67	20.16
3575	123.9	542.1	21.91	1.18	0.41	1.44	20.47	3964	198.4	586.0	21.87	1.62	0.59	1.32	20.55
3599	235.4	543.9	21.92	1.45	0.35	2.10	19.82	4002	243.5	590.3	21.09	1.23	0.52	1.30	19.79
3609	254.0	545.0	21.92	1.44	0.23	1.33	20.59	4026	581.6	593.2	21.98	1.73	0.66	1.60	20.38
3625	457.0	546.9	21.92	1.32	0.82	1.76	20.16	4044	443.4	595.3	21.93	1.36	0.93	1.95	19.98
3633	76.3	547.8	21.98	1.31	1.03	1.86	20.12	4071	383.0	598.3	21.59	1.51	0.40	0.50	21.10
3657	236.2	550.4	21.95	1,53	0.65	1.62	20.34	4084	252.4	600.2	20.77	0.57	0.48	1.02	19.75
3661	184.1	551.0	21.51	1.25	0.54	1.44	20.07	4109	114.0	602,8	21.61	1.25	0.72	1.63	19.98

Star	X	Y	V	(B-V)	(V-R)	(V-I)	I	Star	X	Y	V	(B-V)	(V-R)	(V-I)	I
4115	408.4	603.2	22.00	1.78	0.75	1.57	20.43	4934	519.8	693.4	21.97	1.70	0.89	1.51	20.47
4134	579.9	605.4	21.83	1.55	0.65	1.57	20.27	4963	622.3	696.5	21.29	1.77	0.87	1.86	19.44
4168	72.1	609.0	21.93	1.51	0.51	1.32	20.61	5020	600.6	704.2	21.74	1.08	1.15	2.20	19.55
4173	53.2	609.4	21,78	1.88	0.87	2.12	19.66	5034	583.8	705.5	17.66	1.22	0.72	1.47	16.19
4176	512.4	609.7	21.67	1.90	0.89	2.01	19.66	5107	342.7	715.3	18.49	0.61	0.32	0.75	17.73
4214	512.9	613.6	21.72	1.47	0.57	1.47	20.25	5114	285.1	716.0	21.65	1.84	0.93	1.29	20.36
4237	187.9	617.1	21.89	1.41	0.56	1.50	20.40	5132	624.1	718.1	19.69	1.08	0.57	1.28	18.42
4275	93.1	622.3	18.63	0.71	0.38	0.87	17.77	5190	445.0	724.1	21.99	1.37	0.66	1.58	20.42
4278	29.7	622.7	21.75	1.15	0.64	1.17	20.58	5197	429.8	724.5	21.84	1.91	1.01	1.62	20.23
4280	312.0	623.2	21.94	1.21	0.72	0.97	20.97	5215	481.1	726.5	21.87	2.30	1.11	2.23	19.65
4285	82.0	623.6	22.00	1.16	0.43	1.04	20.96	5288	370.2	736.2	21.92	1.63	0.87	2.10	19.83
4374	562.5	633.8	21.60	1.58	0.72	1.62	19.99	5289	57.6	736.2	21.68	1.85	0.64	2.34	19.34
4390	419.5	635.5	21.88	1.55	0.74	1.18	20.71	5297	235.8	737.6	16.62	0.88	0.44	0.95	15.67
4391	279.4	635.6	21.88	1.39	0.65	2.23	19.64	5397	180.2	750.8	18.54	0.77	0.39	0.89	17.65
4432	337.9	639.3	21.90	1.44	0.56	1.05	20.86	5422	332.0	754.1	21.70	1.36	0.64	1.50	20.21
4456	373.5	641.5	21.56	1.67	0.75	1.66	19.91	5445	420.5	759.3	21.61	1.20	0.70	1.34	20.26
4477	229.7	644.5	21.92	1.38	1.31	2.10	19.83	5460	272.5	761.8	21.99	1.49	0.85	1.27	20.73
4530	418.6	650.4	22.00	1.39	0.60	1.42	20.58	5493	316.9	767.1	21.96	1.35	0.69	1.61	20.35
4549	585.1	652.9	21.96	1.77	0.77	1.59	20.38	5494	507.5	767.2	21.51	1.99	0.86	1.83	19.69
4578	411.3	655.7	21.94	1.41	0.85	1.50	20.44	5538	324.7	774.2	21.78	1.62	1.01	1.40	20.39
4584	403.5	656.4	21.60	1.15	0.19	1.52	20.08	5544	245.4	775.3	21.95	1.36	0.65	1.33	20.63
4652	392.2	663.7	21.99	1.83	0.75	2.03	19.97	5551	274.1	776.6	22.00	1.55	0.80	1.79	20.21
4660	101.6	665.0	21.86	1.77	0.76	1.70	20.16	5564	131.6	778.9	21.54	1.63	0.62	1.51	20.03
4667	110.5	665.8	20.45	1.12	0,53	1.17	19.28	5596	398.9	783.0	20.22	1.65	0.96	2.31	17.91
4689	47.4	668.3	21.11	0.46	0.23	0.65	20.46	5601	466.4	784.0	21.42	1.75	0.80	1.72	19.70
4729	420.1	673.1	21.95	1.44	0.68	1.62	20.34	5610	433.6	785.9	21.82	2.26	0.77	2.31	19.51
4746	339.2	675.2	21.86	1.30	1.05	1.54	20.32	5683	209.0	798.5	21.02	0.68	0.34	0.49	20.54
4789	489.8	679.3	21.11	1.67	0.94	2.39	18.72	5717	444.8	804.0	21.94	1.48	0.67	1.14	20.82
4902	338.7	690.9	21.77	2.04	1.19	2.11	19.67	5753	268.4	810.1	21.77	1.43	0.73	1.46	20.31
4906	608.5	691.2	21.73	2.04	0.70	1.83	19.90	5829	292.3	825.3	21.96	1.40	0.68	1.47	20.50
5895	446.6	840.1	21.92	1.37	0.68	1.32	20.60	6139	437.7	899.9	18.37	1.13	0.58	1.26	17.11
5963	435.1	854.2	21.91	1.31	0.80	1.67	20.24	6208	301.9	921.8	17.06	0.87	0.46	0.97	16.09
5998	70.3	860.3	20.51	1.37	0.75	1.67	18.84	6231	308.7	929.8	19.49	0,95	0.43	1.00	18.50
6019	15.2	864.8	18.92	0.77	0.37	0.87	18.06	6254	453.1	936.4	21.31	1.78	0.89	2.24	19.08
6077	64.5	883.4	16.50	0.79	0.41	0.86	15.64	6264	451.8	939.6	21.98	1.49	0.63	1.59	20.40

TABLE 3b. Blue stars $((B-V) < 0.6)$ in NGC 185

Star	X	Y	V	(B–V)	(V–R)	(V–I)	I	Star	X	Y	V	(B–V)	(V–R)	(V–I)	I
3116	428.8	502.4	19.75	0.41	0.09	0.43	19.32	3511	416.8	535.1	22.24	0.53	0.79	1.77	20.46
5370	308.2	747.4	20.45	-0.14	,-0.50	—	—	3410	307.1	527.0	22.26	0.48	0.16	1.68	20.59
628	387.3	202.3	20.62	0.44	0.26	0.45	20.18	4553	102.6	653.3	22.36	0.43		1.27	21.09
4084	252.4	600.2	20.77	0.57	0.48	1.02	19.75	2770	470.4	468.6	22.36	0.18	—·	0.98	21.38
1839	318.8	362.8	20.88	0.49	0.09	0.86	20.02	2502	373.5	440.1	22.37	0.53	0.81	—	—
2244	413.1	409.2	20.99	0.59	0.35	1.16	19.83	3465	329.5	531.4	22.37	0.45	—	1.32	21.06
3095	297.9	500.7	21.07	0.13	0.06	0.48	20.60	3408	299.9	526.8	22.37	0.32	·	1.74	20.63
4689	47.4	668.3	21.11	0.46	0.23	0.65	20.46	3320	222.9	519.2	22.40	0.47	0.38	——	—
1428	219.0	315.3	21.24	0.43	0.18	0.40	20.84	668	244.2	210.3	22.42	0.06			—
315	457.3	126.6	21.27	0.34	0.03	0.39	20.88	3068	378.9	497.6	22.45	0.29	—-	1.65	20.80
2893	365.2	480.1	21.28	0.20	-0.07	0.12	21.16	4388	276.6	635.4	22.48	0.60	—		—
1750	247.6	352.5	21.30	0.58	0.34	0.99	20.31	2367	248.4	424.7	22.49	0.34	—	1.79	20.70
3187	355.6	508.4	21.54	-0.24	0.40	1.98	19.55	2949	349.6	485.9	22.51	0.29	0.25	0.91	21.60
2588	366.6	449.0	21.54	0.05	-0.19	—	—	1372	586.6	310.2	22.51	0.19	0.45	1.48	21.03
3296	152.8	517.7	21.63	-0.49	0.23	—	—	4908	511.4	691.5	22.52	0.51	—	—-	—
3102	386.2	501.2	21.63	0.47	0.85	0.39	21.25	3672	341.4	552.7	22.52	0.56	—-	1.52	21.00
2966	341.1	487.6	21.80	0.43	--	1.68	20.11	2891	355.7	480.0	22.54	0.48	—-		—
3219	391.0	511.3	21.84	0.36	0,00	0.69	21.16	3900	43.2	578.7	22.66	0.60	—	1.45	21.21
5907	596.7	843.3	21.88	0.12	--	--	--	3230	317.3	511.9	22.67	-0.26	—		—
3052	373.4	496.4	21.94	-0.24	—	—	—	3172	436.0	507.3	22.67	0.45	—-	-	—
4298	496.7	625.3	21.95	-0.27	0.07	—	—	3038	365.4	494.5	22.70	-0.36	1.27	—-	
3211	372.5	510.5	21.95	0.48	0.08	2.48	19.47	1816	321.2	359.9	22.71	0.26	—-		—-
2882	344.5	479.3	21.97	0.59	0.30	—	—	2317	305.4	418.5	22.72	0.44	—	2.16	20.55
3474	402.3	532.3	22.00	0.37	0.27	0.79	21.22	4483	281.8	645.0	22.76	0.60	—-	1.39	21.37
3658	397.0	550.4	22.06	0.36	0.75	—	—	5313	245.0	739.4	22.76	-0.66	—	—-	—
3036	414.4	494.4	22.06	0.58	0,86	1.96	20.09	2976	364.3	488.5	22.78	-0.24	—-	—	—
3729	475.7	558.7	22.11	0.40	0.25	—	—	3745	53.3	560.7	22.78	-0.13	—	—	—
3194	349.5	508.8	22.17	0.23	0.35	—	—	2995	404.1	490.6	22.78	0.13	—	—-	—-
3251	373.4	513.8	22.18	0.57	—	—	—	949	253.1	258.8	22.78	0.37	0.77	1.10	21.68
2486	367.9	438.4	22.18	0.02	0.60	2.08	20.09	2597	155.8	449.7	22.80	0.16	—	1.48	21.32
3182	440.2	508.0	22.81	0.26	—	—	—	3284	434.3	516.4	23.15	0.25	—-	—	—-
3459	492.9	530.9	22.82	0.39	—	—	—	3701	59.6	556.3	23.18	0.34	—-	—	
2615	370.3	451.2	22.83	0.29	—	—	—	1769	274.2	354.8	23.27	0.41	—-	—-	
3523	412.3	536.3	22.84	-0.27	—	1.40	21.43	2073	269.4	389.8	23.28	0.57	—-	1.45	21.82
2611	362.0	450.8	22.85	0.32	—	—	—	3350	443.0	521.8	23.31	-0.55		—-	
3007	440.1	491.6	22.93	0.19	—	—	—	4397	354.3	636.0	23.35	0.00	—-	1.90	21.44
3644	327.1	549.3	22.97	0.24	—	2.19	20.77	2594	185.7	449.3	23.38	0.57	—	1.86	21.51
3932	303.3	581.5	23.03	0.56	—	1.11	21.92	1201	381.8	290.6	23.45	0.59	—	—	
3565	328.1	541.1	23.05	0.38	—	1.56	21.48	1506	380.8	324.4	23.50	0.54	—-		—-
4724	310.8	672.4	23.10	0.43	1.19	2.21	20.89	2673	397.4	457.5	23.62	-0.37			—
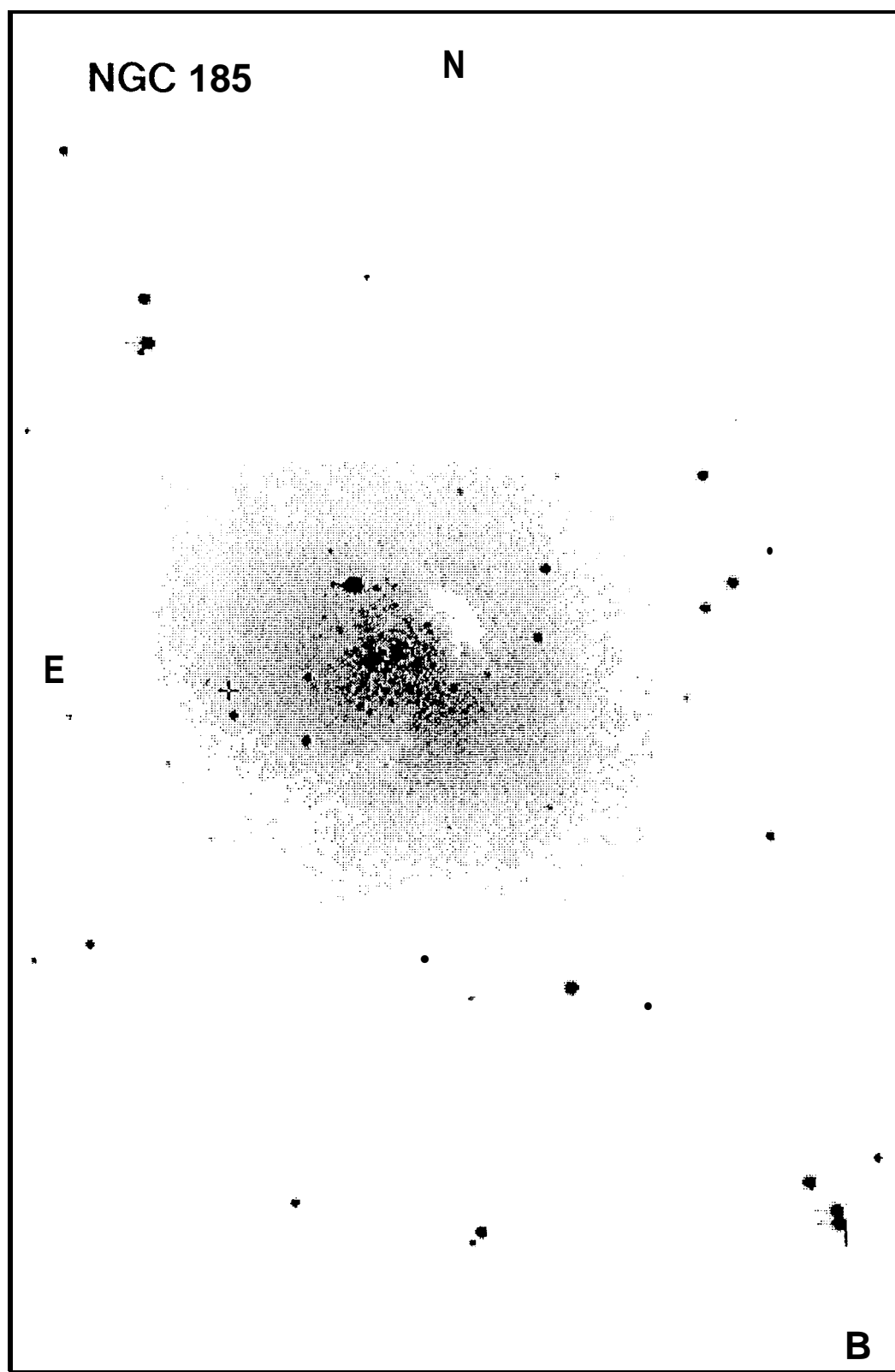
NGC 185

N

E

B

Fig 1(a) (Lee et al)

NGC185

N

E

V

Fig 1(b) (Lee et all)

NGC185

N

E

Fig 1 (c) (Lee et al)

NGC 1.85 (V<22)

Fig. 2(a) (Lee et al.)

NGC185 (1 3 −V<0.6)

Fig 2(b) (Lee et al)

Figure axis labels:
- Y-axis: Y(px=0.205") E, values 0, 200, 400, 600, 800, 1000
- X-axis: X(px=0.205") S, values 600, 4-00, 200, 0
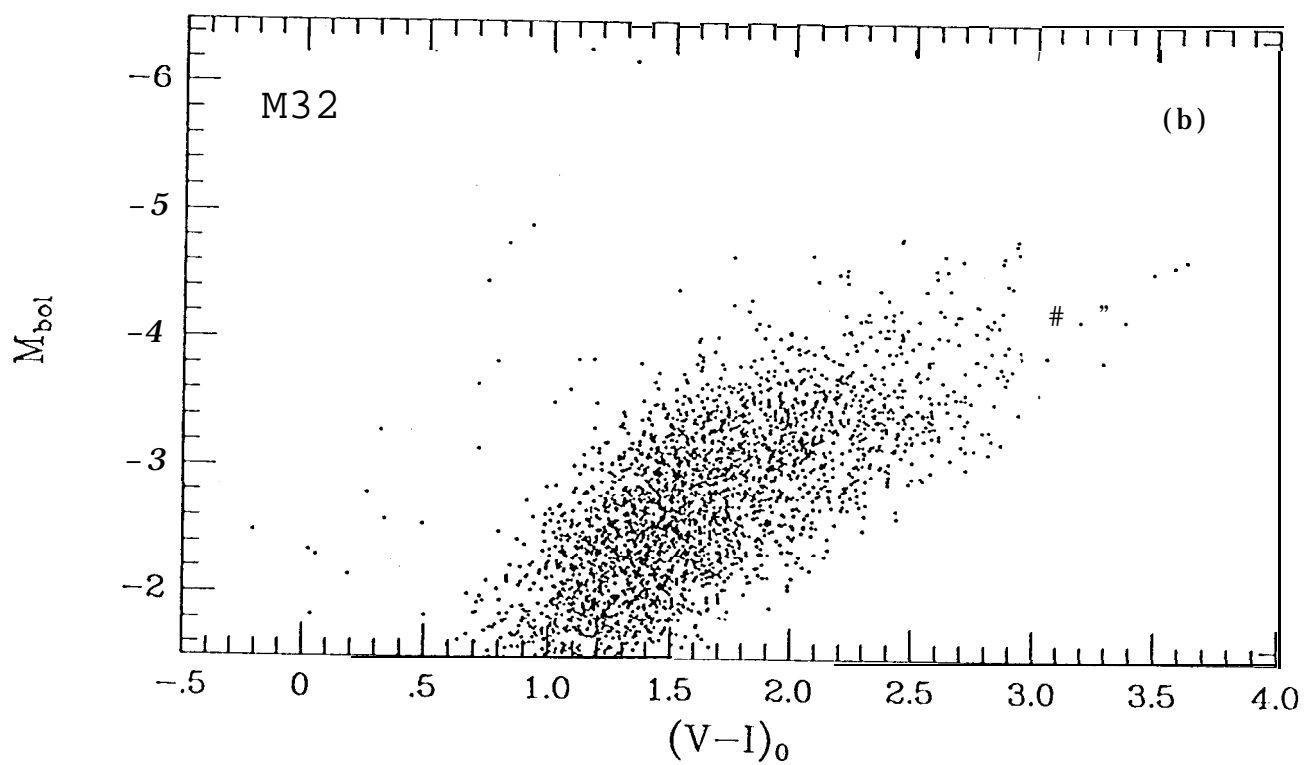
Point labels: 0628, 1839, 02244, 3116, 4084, 5370

NGC 185 (17.5 <1<20, 1.4<V−I)
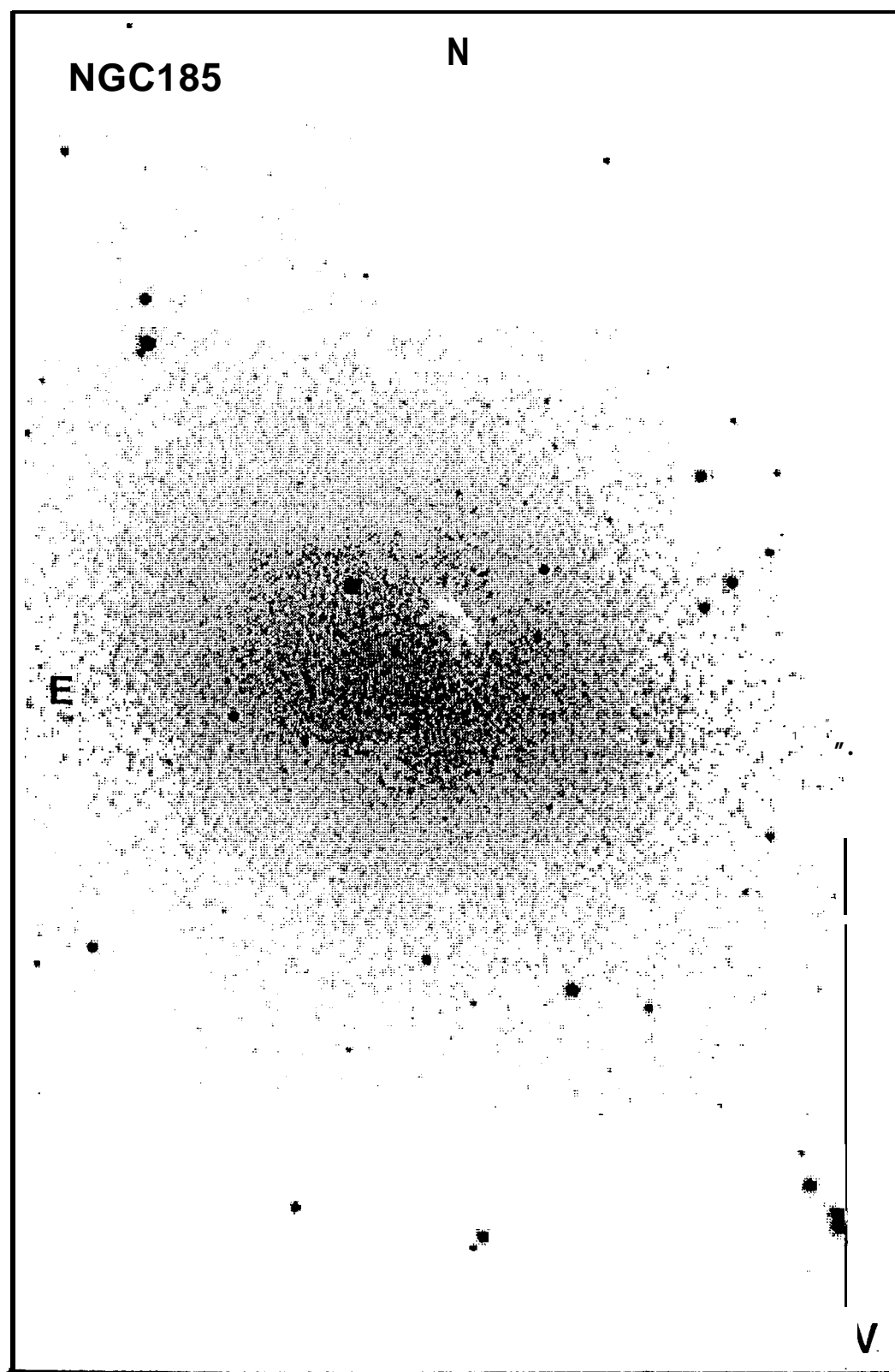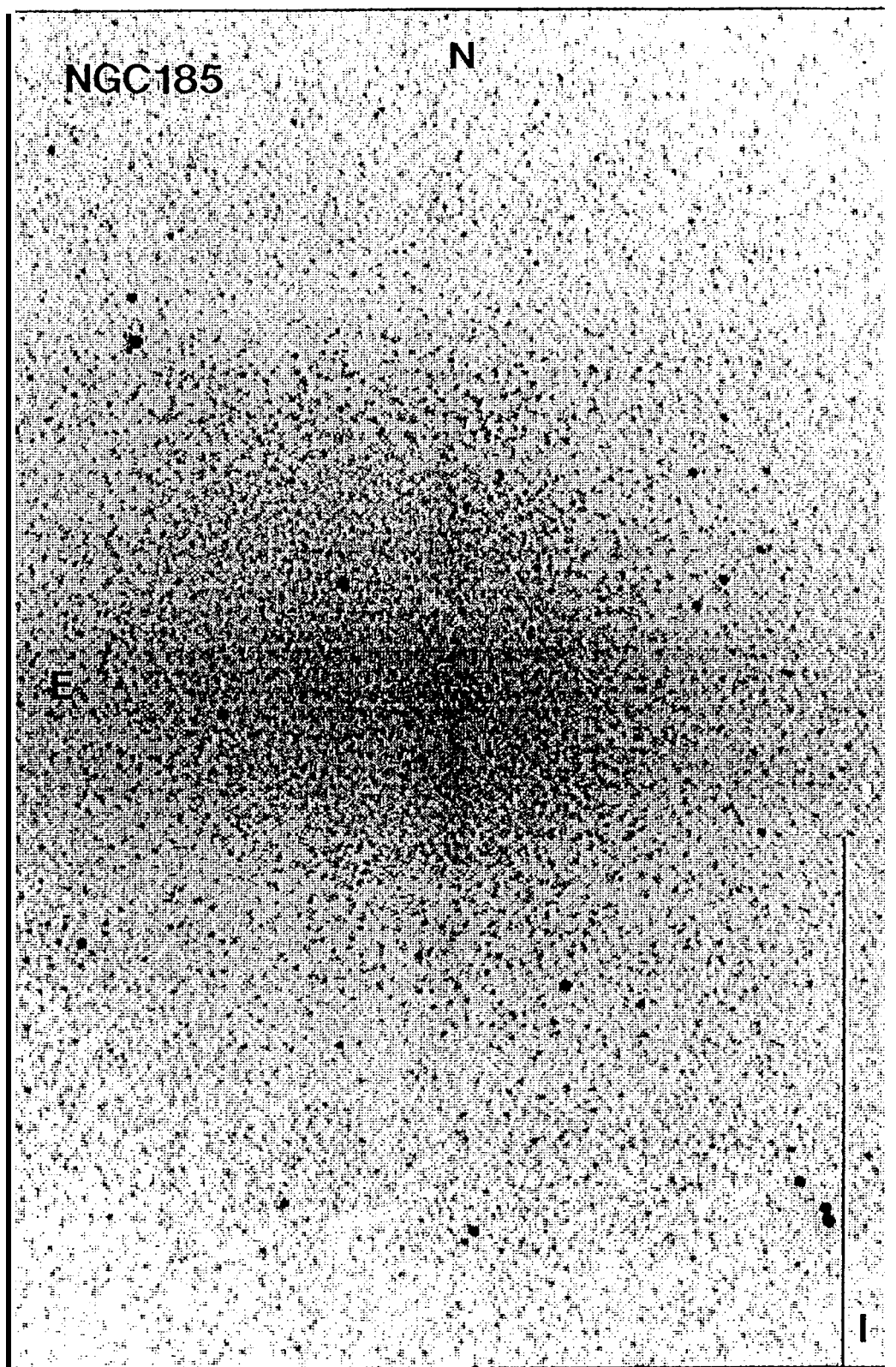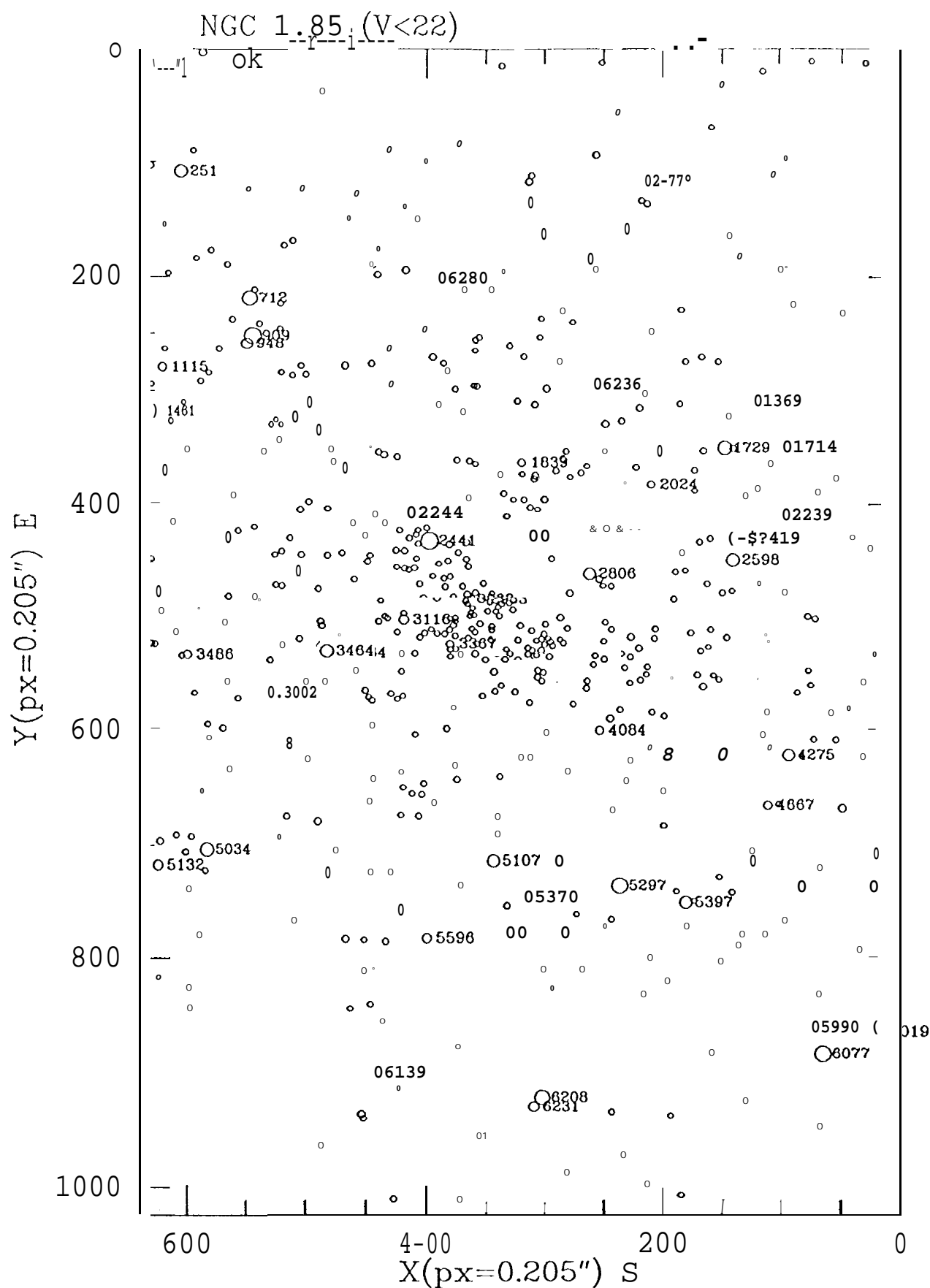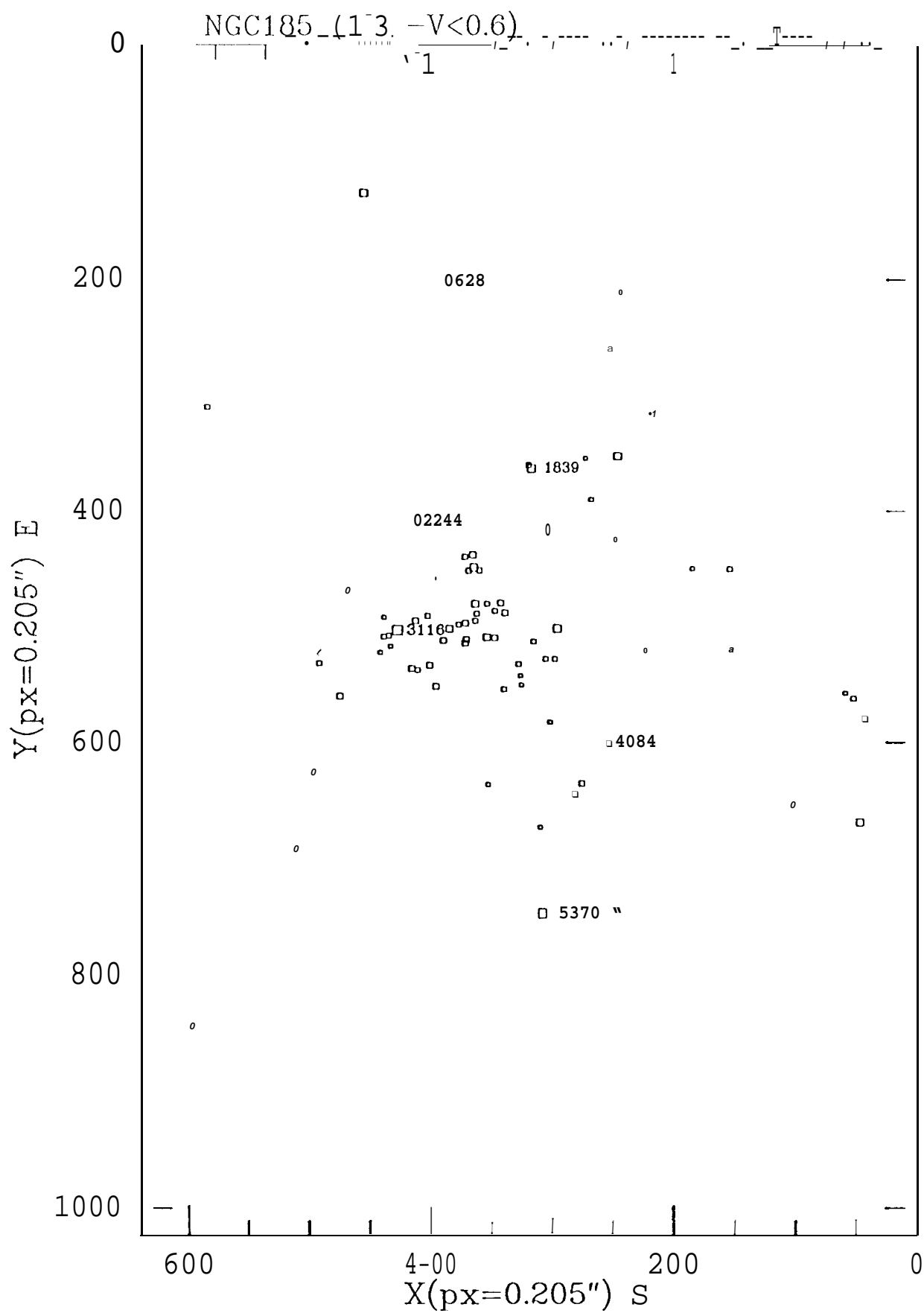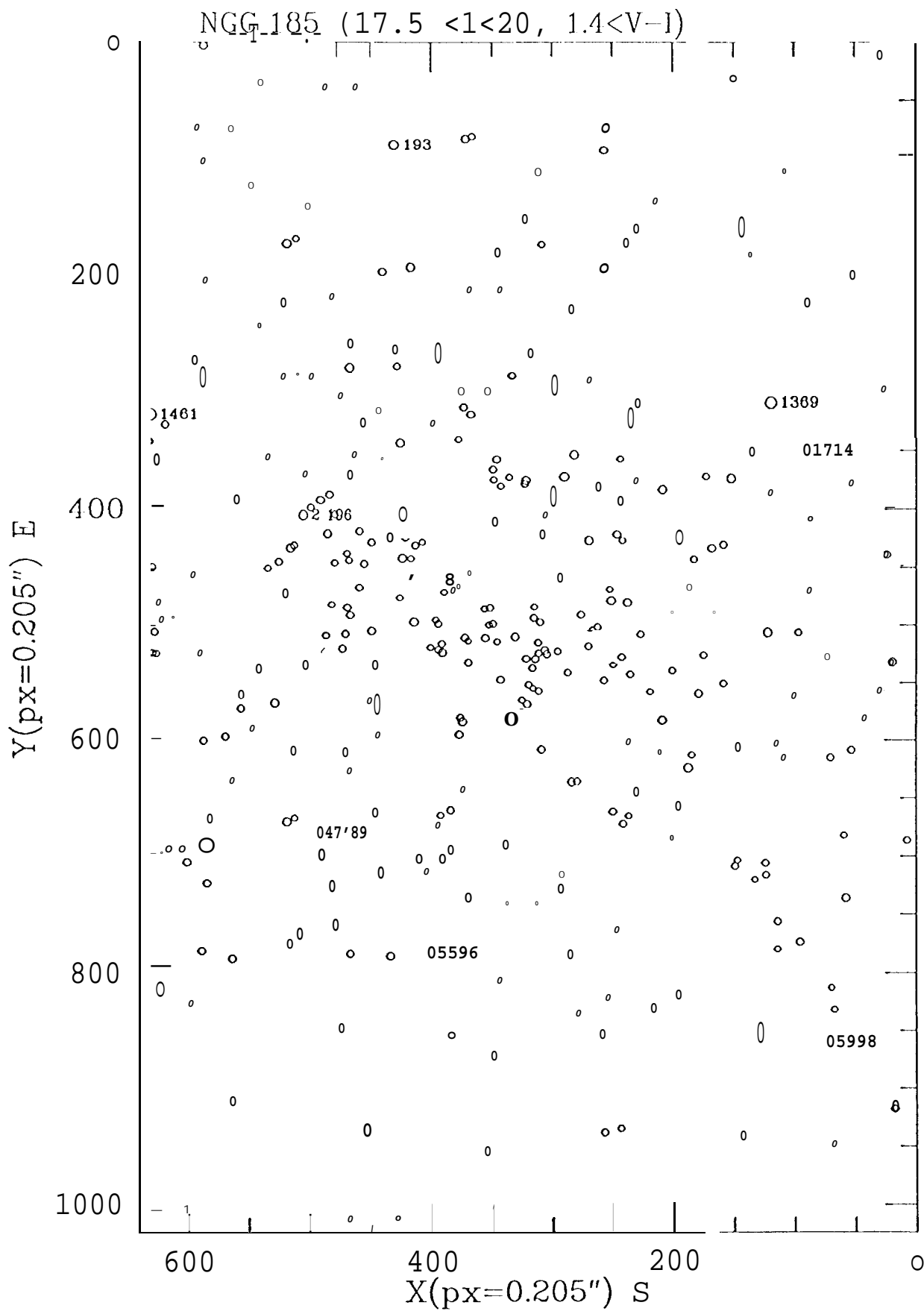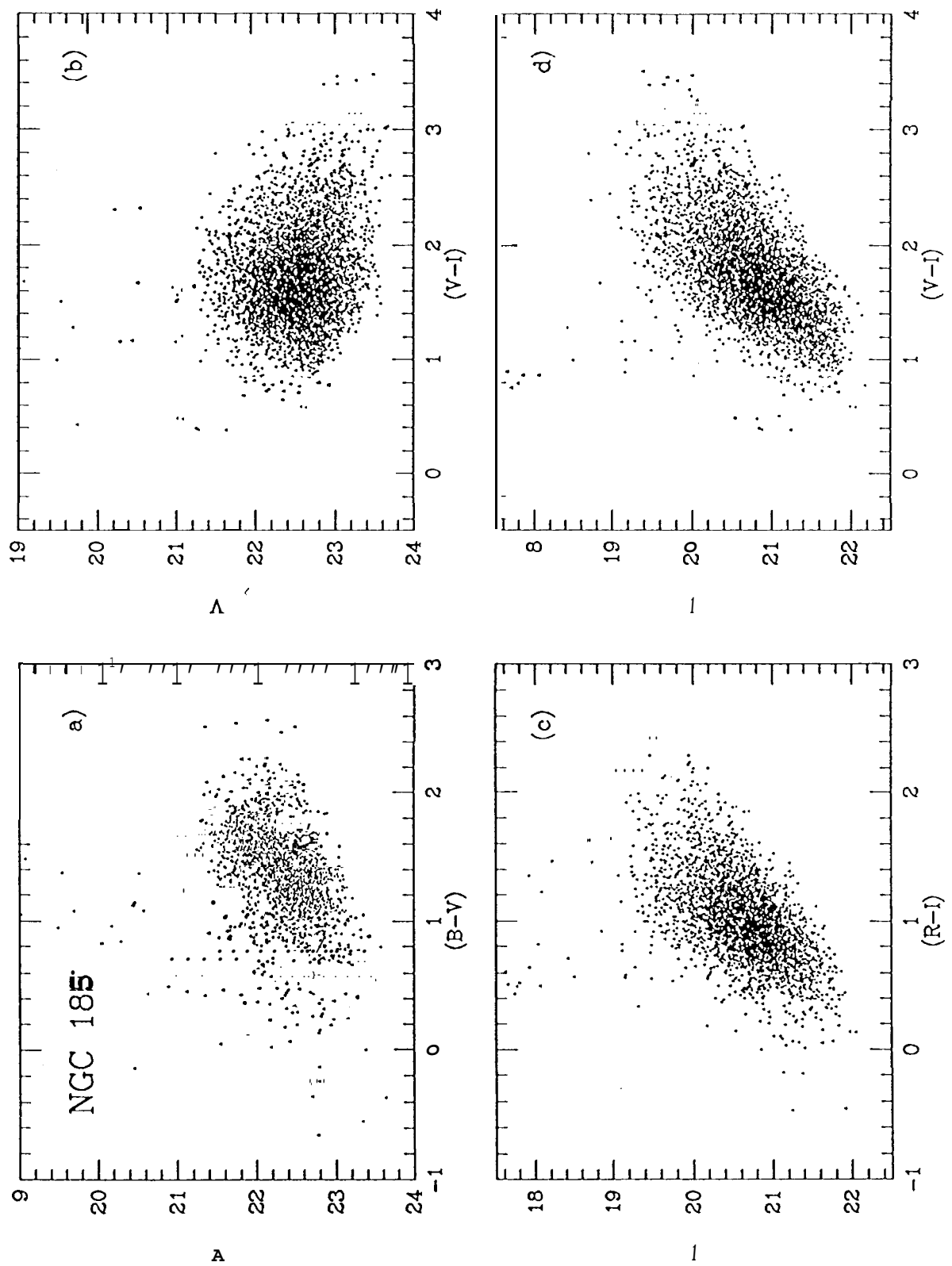
Fig. 3 (Lee et al.)

Fig. 4 (Lee et al.)

M15, M2, NGC 85.., 47Tuc

(V−I)

I
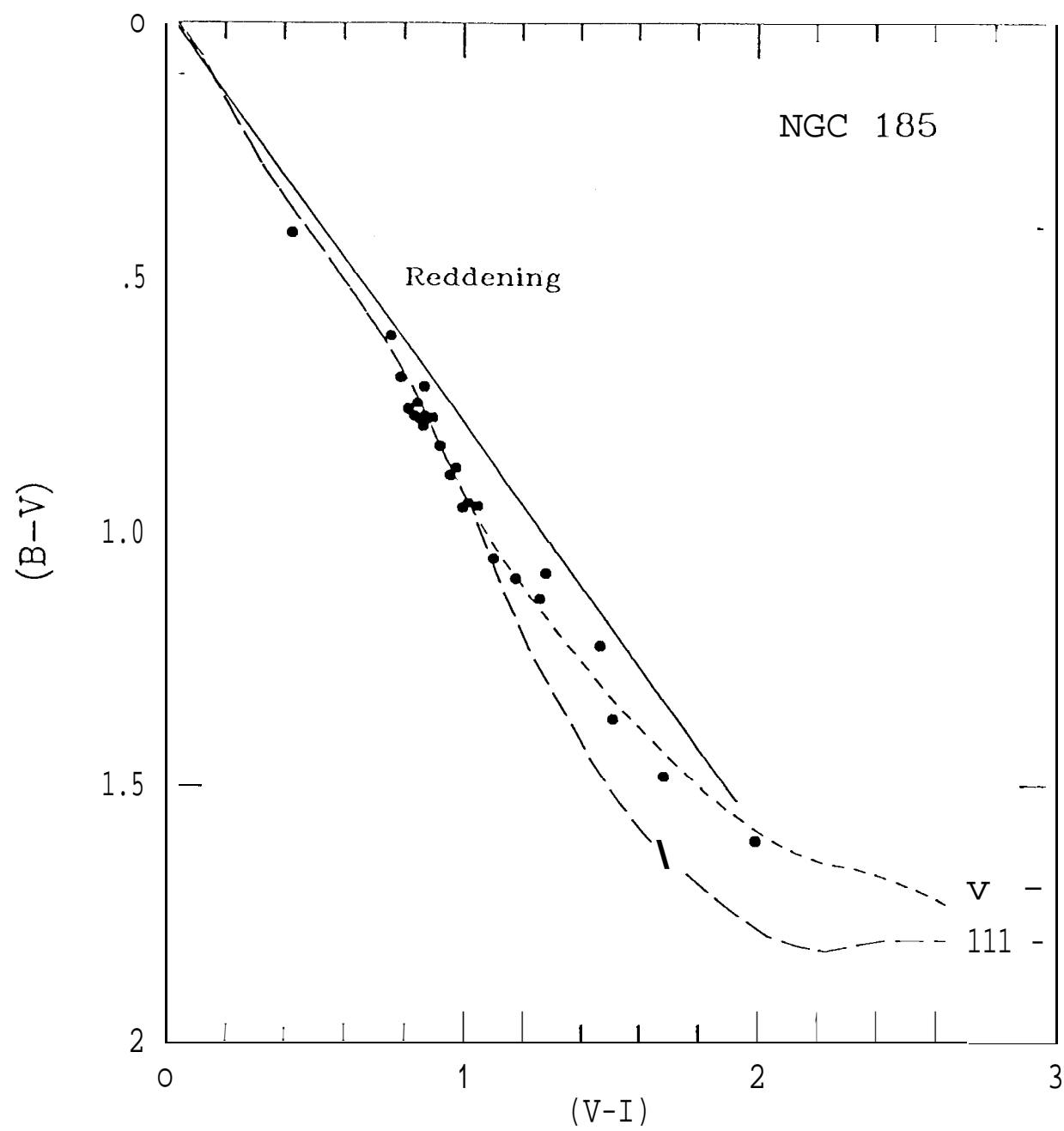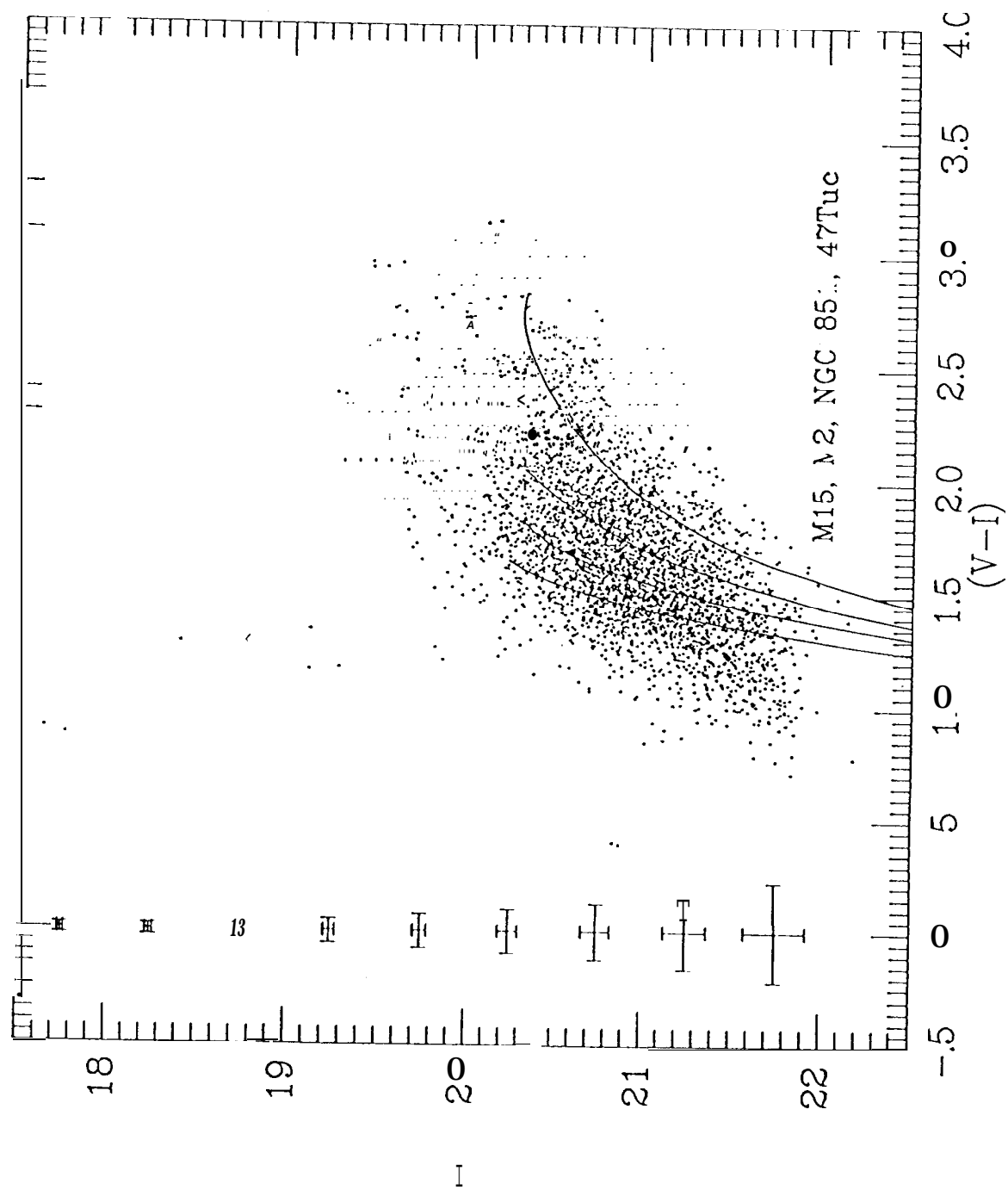
Fig. 5 (Lee et al.)
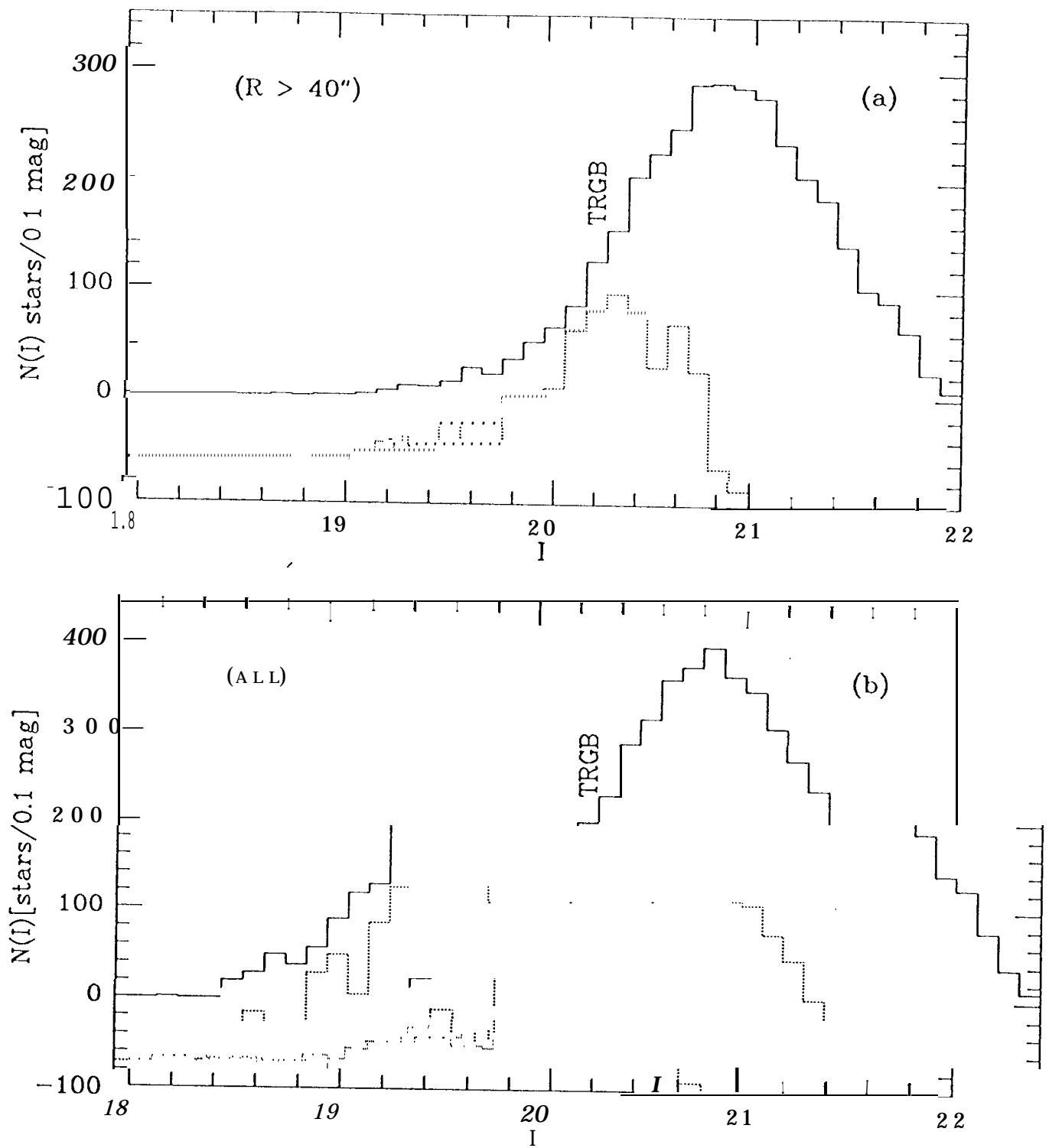
Fig. 6 (Lee et al.)
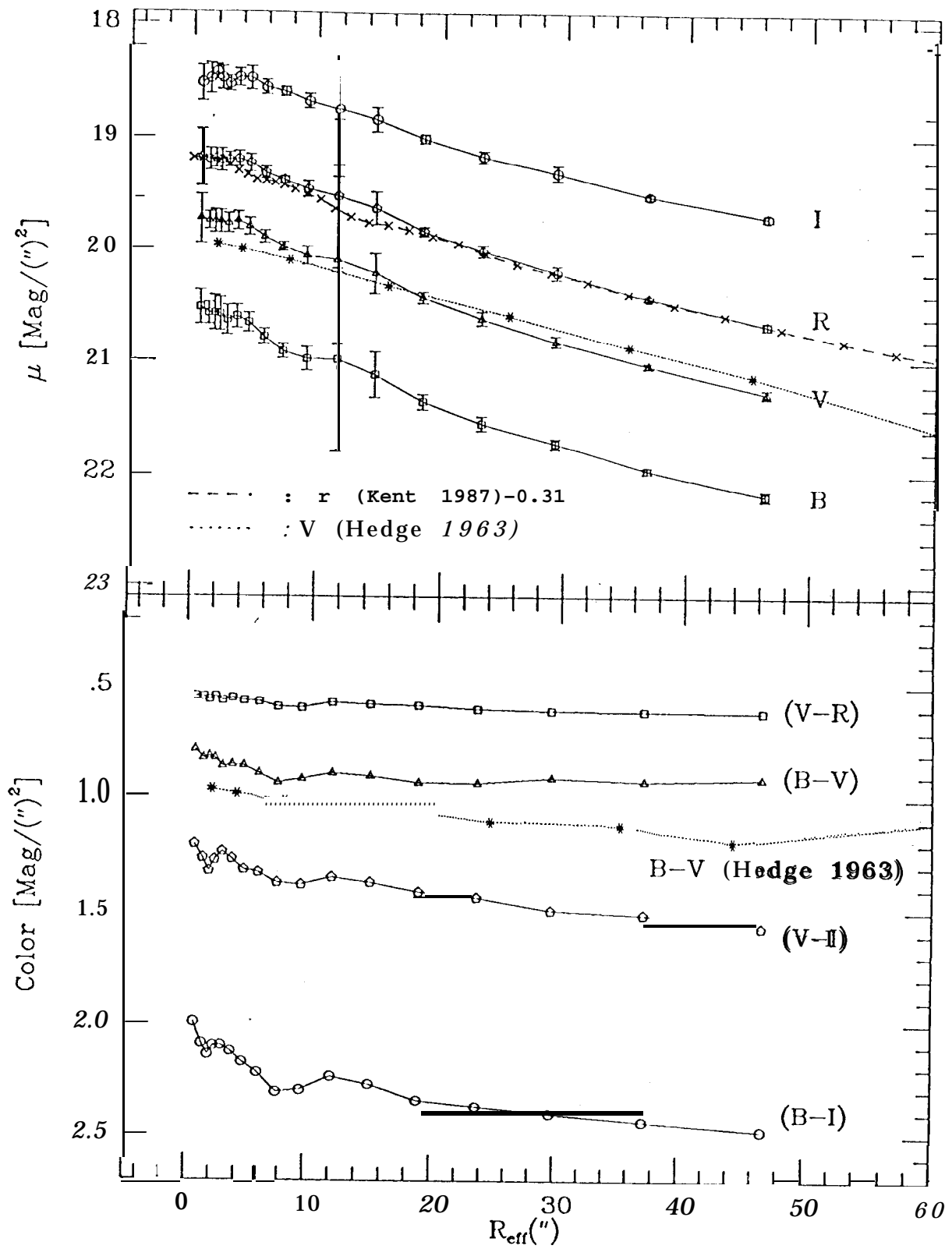
Fig. 7a (Lee et. al.)
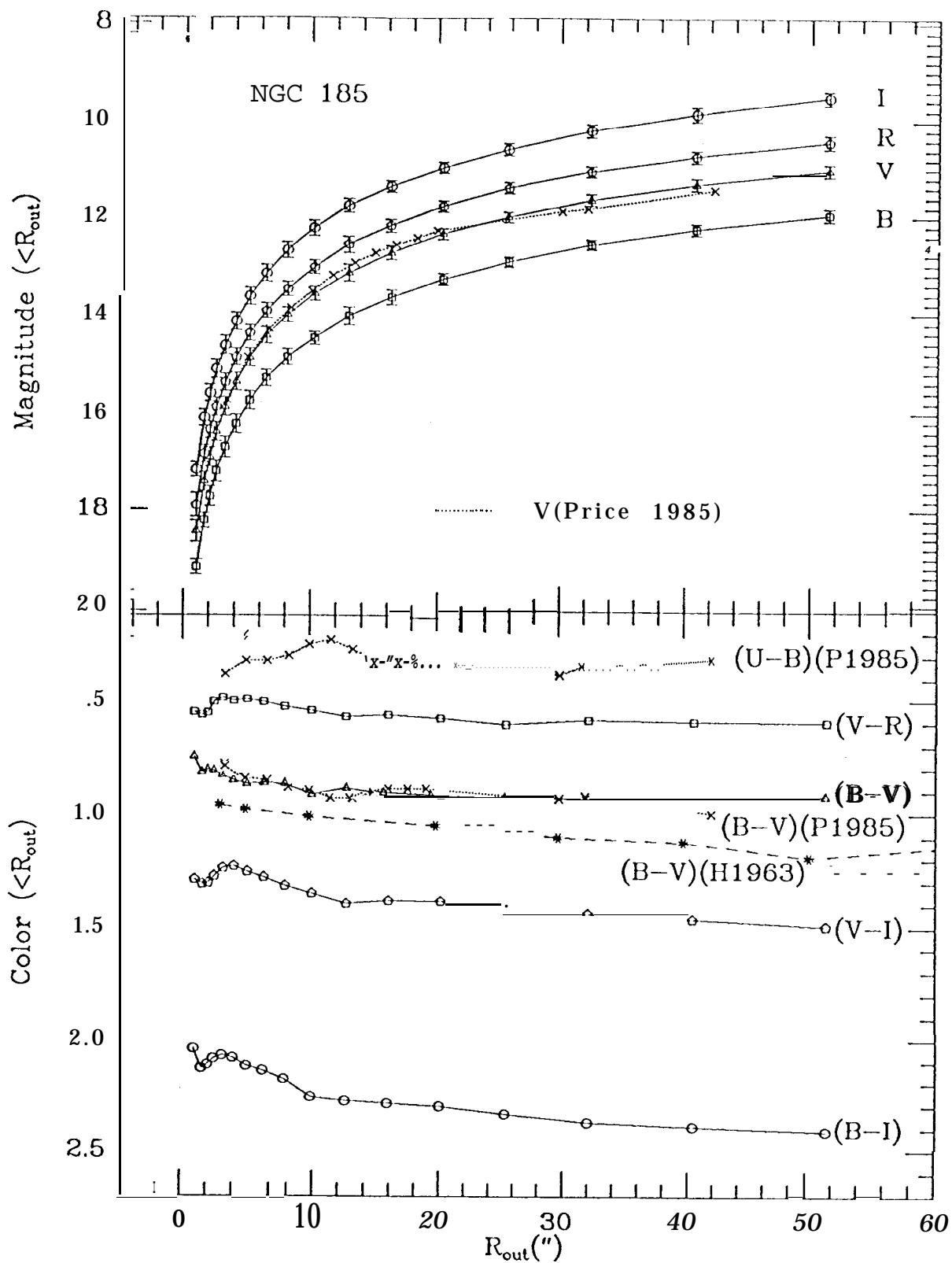
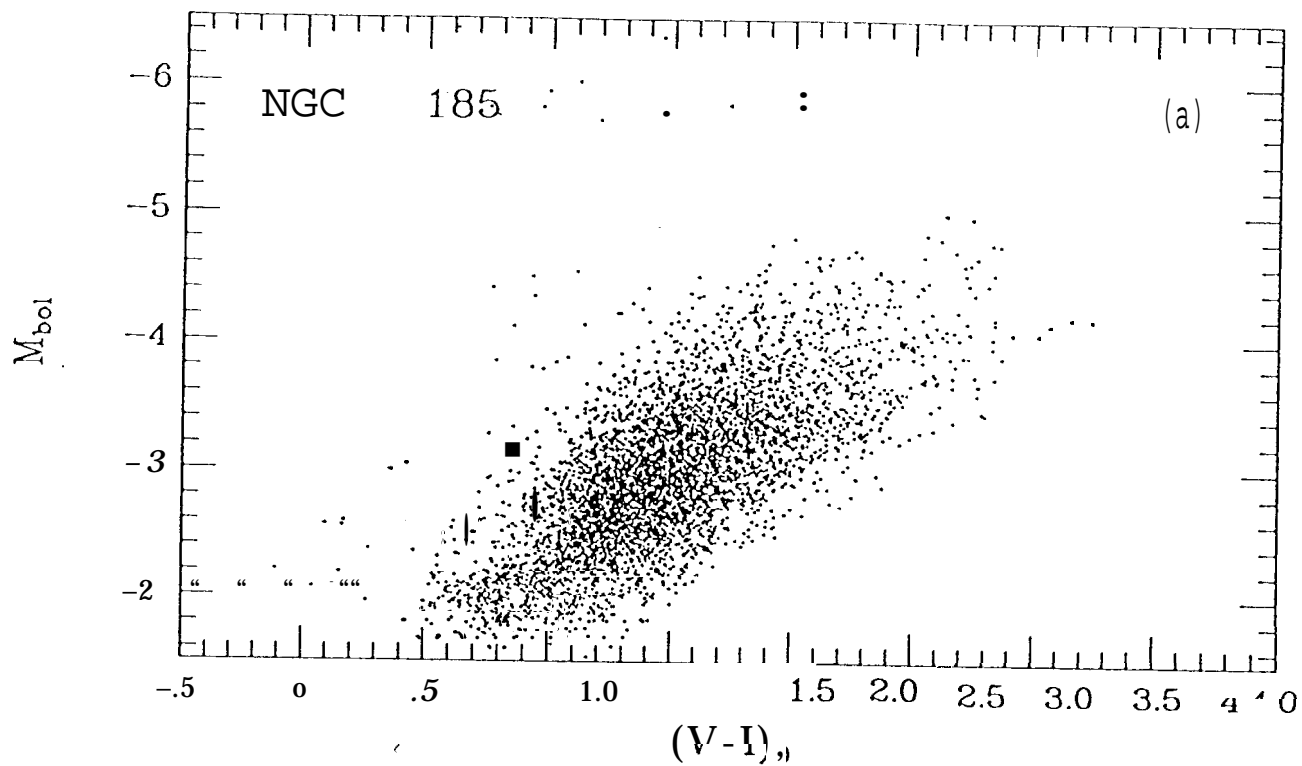Fig. 7b (Lee et al.)
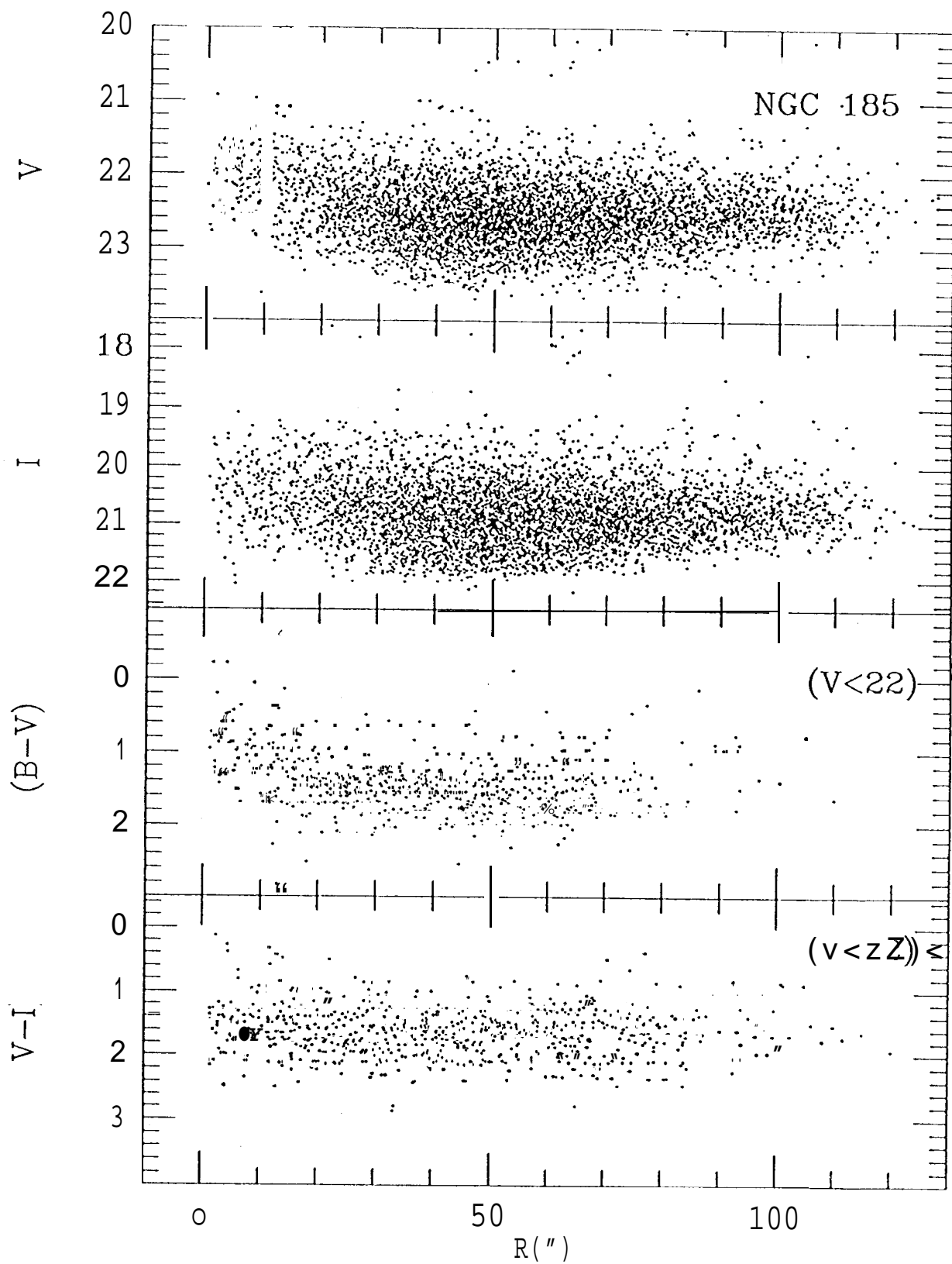
Fig. 8 (Lee et al.)
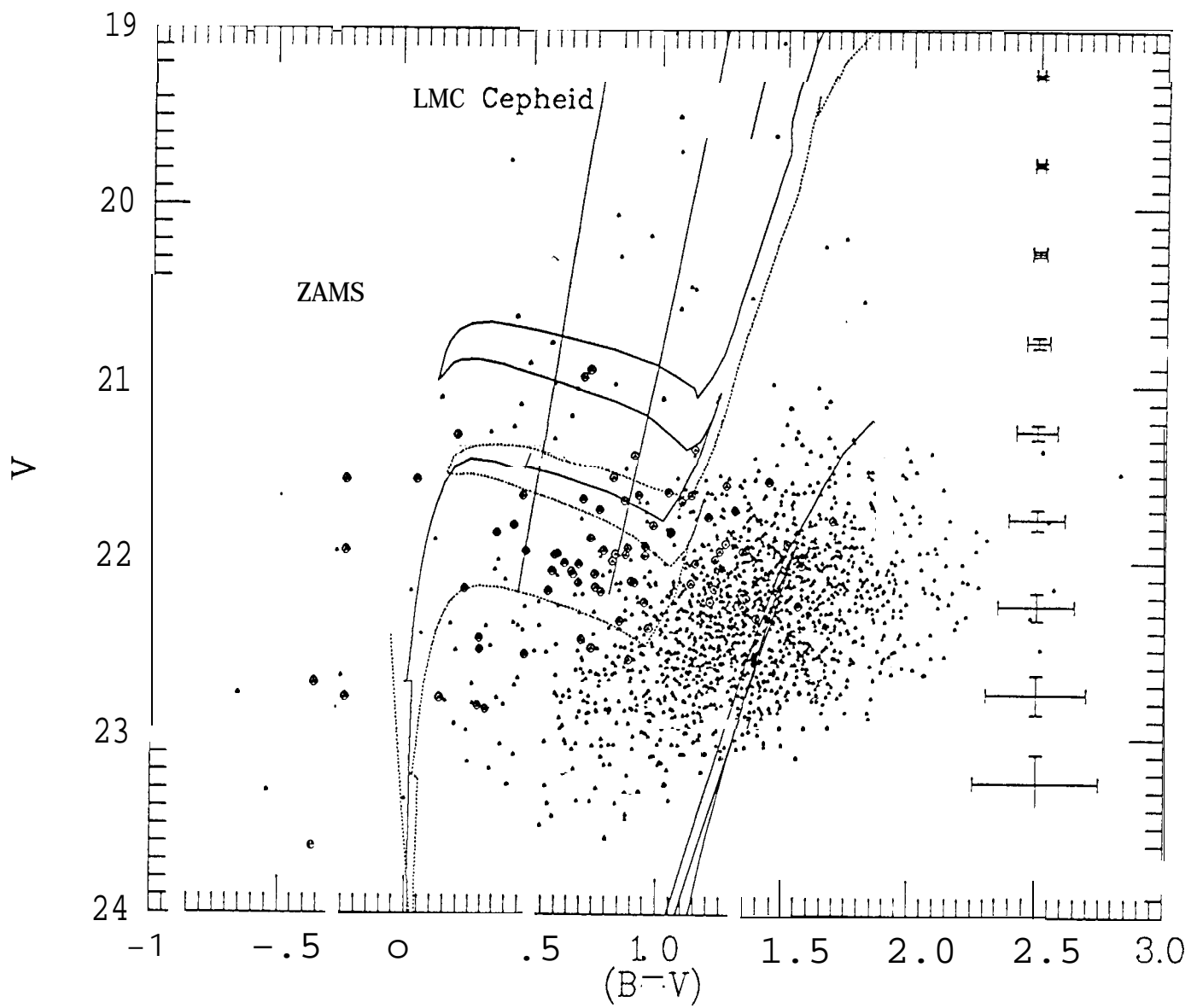
Fig. 9 (Lee et al.
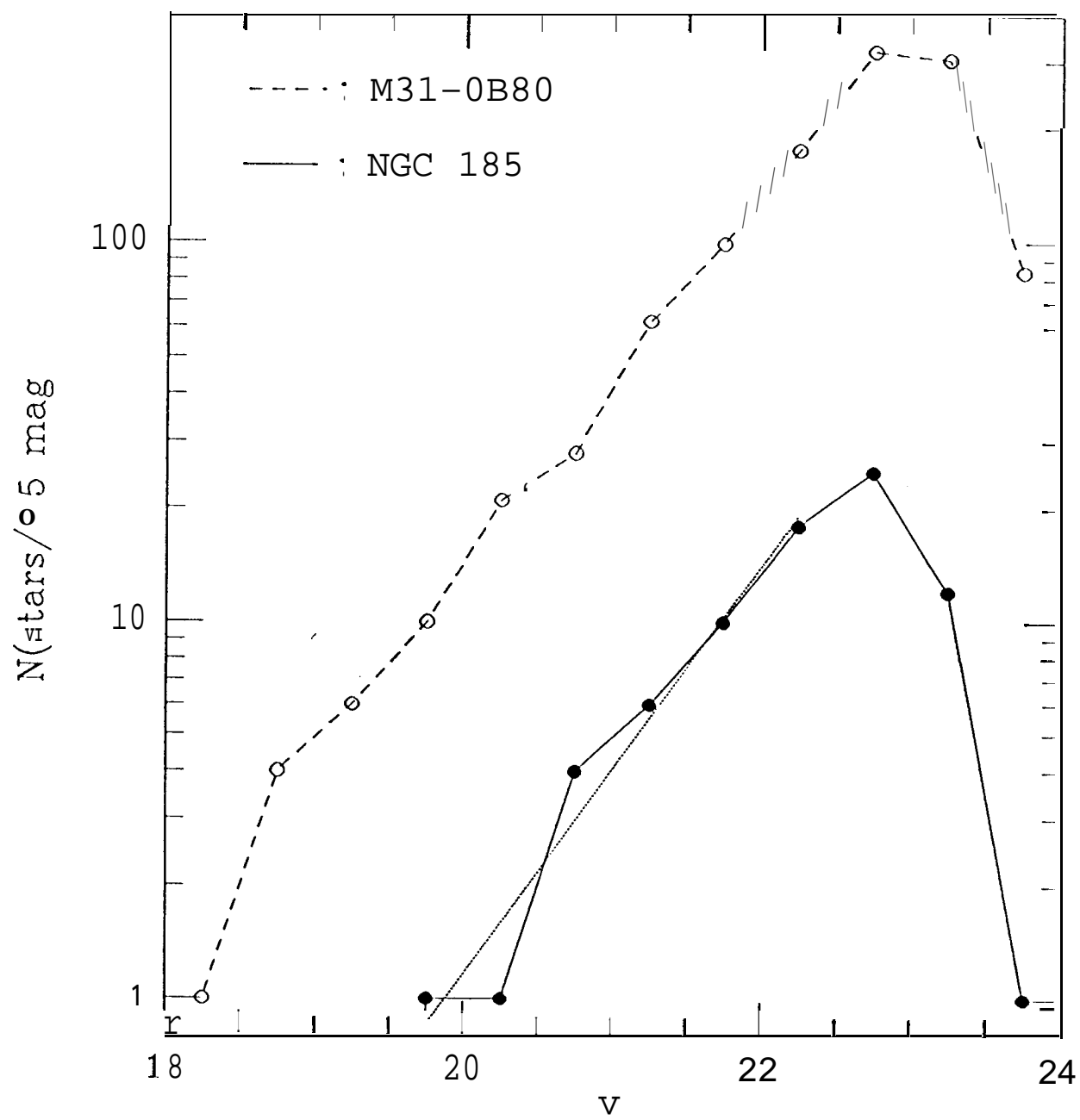
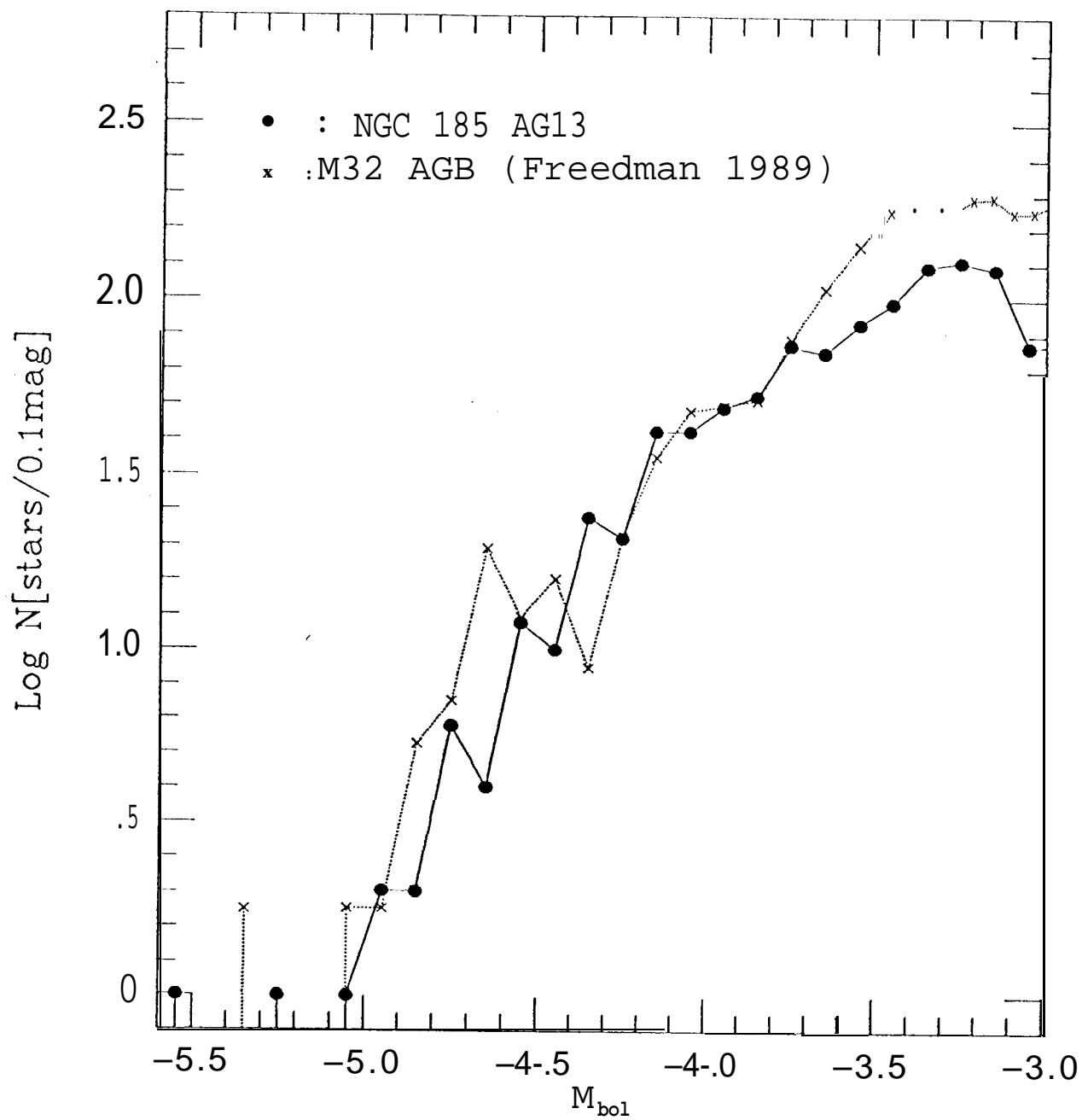Fig. 10 (Lee et al.)
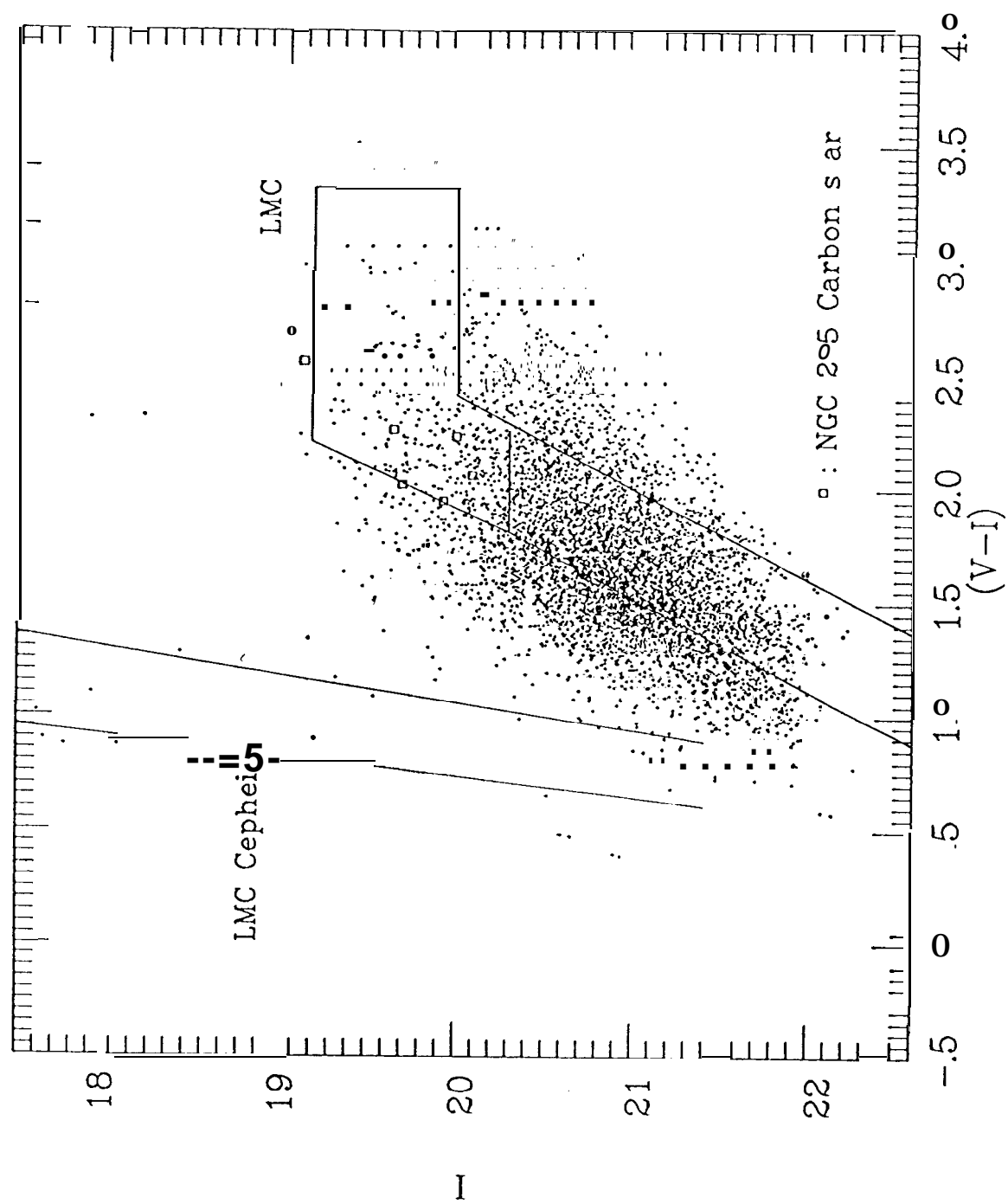
Fig. 11 (Lee et al.)

Fig. 12 (Lee et al.)

Fig. 13 (Lee et al.)